Title

SlERF52 Regulates SlTIP1;1 Expression to Accelerate Tomato Pedicel Abscission

Permalink

https://escholarship.org/uc/item/7zz203dr

Journal

Plant Physiology, 185(4)

ISSN

0032-0889

Authors

Wang, Rong
Li, Ruizhen
Cheng, Lina
et al.

Publication Date

2021-04-23

DOI

10.1093/plphys/kiab026

Peer reviewed

doi:10.1093/plphys/kiab026 PLANT PHYSIOLOGY 2021: 0: 1–18

Plant Physiology

Research Article

SlERF52 regulates *SlTIP1;1* expression to accelerate tomato pedicel abscission

Rong Wang,[1,2] Ruizhen Li,[1,2] Lina Cheng,[1,2] Xiaoyang Wang,[1,2] Xin Fu,[1,2] Xiufen Dong,[1,2] Mingfang Qi,[1,2] Caizhong Jiang ,[3,4] Tao Xu [1,2,*,†] and Tianlai Li[1,2,†]

1 College of Horticulture, Shenyang Agricultural University, Shenyang, Liaoning 110866, People's Republic of China
2 Key Laboratory of Protected Horticulture of Ministry of Education, Shenyang, Liaoning Province, China
3 Crops Pathology and Genetic Research Unit, United States Department of Agriculture Research Service, California, USA
4 Department of Plant Sciences, University of California, California, USA

*Author for communication: syauxutao@syau.edu.cn
[†]Joint senior authors.

T.X. and T.L. conceived the original screening and research plans; T.X. and T.L. supervised the experiments; T.X. and T.L. designed the research; R.W., X.W., R.L., M.Q., X.F., and X.D. performed the experiments; T.X., T.L., and C.J. conceived the project and wrote the article with the contributions of all authors; and T.X. and T.L. agreed to serve as the authors responsible for contact and correspondence.

The author responsible for distribution of materials integral to the findings presented in this article in accordance with the policy described in the Instructions for Authors (https://academic.oup.com/plphys) is: Tao Xu (syauxutao@syau.edu.cn).

Abstract

Abscission of plant organs is induced by developmental signals and diverse environmental stimuli and involves multiple regulatory networks, including biotic or abiotic stress-impaired auxin flux in the abscission zone (AZ). Depletion of auxin activates AZ ethylene (ETH) production and triggers acceleration of abscission, a process that requires hydrogen peroxide (H_2O_2). However, the interaction between these networks and the underlying mechanisms that control abscission are poorly understood. Here, we found that expression of tonoplast intrinsic proteins, which belong to the aquaporin (AQP) family in the AZ was important for tomato (*Solanum lycopersicum*) pedicel abscission. Liquid chromatography–tandem mass spectrometry and in situ hybridization revealed that *SlTIP1;1* was most abundant and specifically present in the tomato pedicel AZ. *SlTIP1;1* localized in the plasma membrane and tonoplast. Knockout of *SlTIP1;1* resulted in delayed abscission, whereas overexpression of *SlTIP1;1* accelerated abscission. Further analysis indicated that *SlTIP1;1* mediated abscission via gating of cytoplasmic H_2O_2 concentrations and osmotic water permeability (P_f). Elevated cytoplasmic levels of H_2O_2 caused a suppressed auxin signal in the early abscission stage and enhanced ETH production during abscission. Furthermore, we found that increasing P_f was required to enhance the turgor pressure to supply the break force for AZ cell separation. Moreover, we observed that SlERF52 bound directly to the *SlTIP1;1* promoter to regulate its expression, demonstrating a positive loop in which cytoplasmic H_2O_2 activates ETH production, which activates *SlERF*52. This, in turn, induces *SlTIP1;1*, which leads to elevated cytoplasmic H_2O_2 and water influx.

Introduction

Plant organ abscission occurs during vegetative and reproductive growth and was triggered by both developmental signals and environmental stimuli (Addicott, 1982). It takes place in specific regions called abscission zones (AZs), which comprise a group of round, specialized meristem-like cells (Wang et al., 2013). Biotic or abiotic stresses reduce basipetal polar transport of the phytohormone auxin from the distal organ (i.e. the flower and fruit) to the AZ. Depletion of

Received October 15, 2020. Accepted January 08, 2021. Advance access publication 28 January 2021

indole-3-acetic acid (IAA) sensitizes the AZ to ethylene (ETH; Meir et al., 2006; Sakamoto et al., 2008; Meir et al., 2010). In tomato (*Solanum lycopersicum*), it has been reported that after auxin levels in the pedicel are depleted (e.g. by flower removal), the expression of five early auxin response *AUX/IAA* genes (*IAA1*, *IAA3*, *IAA4*, *IAA7*, and *IAA10*) decreases rapidly and the expression levels of *IAA8* and *IAA9* decrease gradually, consistent with reduction of the auxin signal in the AZ (Meir et al., 2010). Recently, *KNOTTED1-LIKE HOMEOBOX PROTEIN 1* (*KD1*) was shown to contribute to the auxin concentration and response gradient in the AZ; *KD1* knockdown lines were reported to delay tomato pedicel abscission (Ma et al., 2015). In addition, it has been shown that in tomato downregulation of the micro-RNA *SlmiR160* that targets the auxin response factors (ARFs) *SlARF10*, *SlARF16*, and *SlARF17* leads to floral organ abscission (Damodharan et al., 2016). Depletion of IAA activates AZ ETH production, which triggers and accelerates abscission. In the tomato pedicel, *1-AMINOCYCLOPROPANE-1-CARBOXYLATE SYNTHASE 1A* (*ACS1A*), *ACS2*, and *ACS6*, combined with *ACC OXIDASE 1* (*ACO1*) and *ACO5*, were found to have upregulated expression during abscission (Meir et al., 2010). Further, *ETHYLENE RESPONSE FACTOR 52* (*ERF52*) was identified as a positive regulator of tomato pedicel abscission (Nakano et al., 2014). Although much research has supported the central role of auxin and ETH in mediating abscission, little is known about the factors involved in the shift from the auxin-sensitive stage to the ETH-sensitive stage.

Oxidative stress and related stress-inducing agents have been noted for their role in auxin antagonism such as inhibiting root elongation and limiting cotyledon and leaf expansion (Chaoui and Ferjani, 2005; Taras et al., 2005; Blomster et al., 2011). Lack of glutathione and thioredoxin disrupts auxin homeostasis and alters development (Bashandy et al., 2010). Reactive oxygen species (ROS) affect auxin response at multiple levels. First, oxidative stress-induced upregulation of peroxidases (Prxs) perturbs auxin homeostasis due to their auxin oxidase activity (Elobeid and Polle, 2012). Second, hydrogen peroxide (H_2O_2) triggers cellular mitogen-activated protein kinase (MAPK) pathways and repress auxin dependent signaling (Kovtun et al., 2000). Third, ROS enhances AUX/IAA stability and, consequently, suppress ARF activity (Blomster et al., 2011). Interestingly, peroxidases, MAPK pathways, and ARF are all reported to be involved in abscission (Henry and Jensen, 1973; Patharkar and Walker, 2015; Damodharan et al., 2016). ROS production occurs mostly in the apoplast and is catalyzed by Nicotinamide adenine dinucleotide phosphate (NADPH)-dependent oxidases (respiratory burst oxidase homologs, RBOHs), which are essential for normal growth and development (Miller et al., 2010). An instant increase in NADPH oxidase (*RBOH*) expression was observed immediately after the flower was removed during tomato pedicel abscission (Bar-Dror et al., 2011). Moreover, H_2O_2 treatment was shown to slightly counteract the inhibitory effects of IAA on "middle old" AZ strip abscissions (Sakamoto et al., 2008).

Furthermore, ROS are also known to be involved in ETH biosynthesis and signaling. During leaf pulvinus, abscission induced via water-deficit stress in Cassava (*Manihot esculenta* Crantz), the enhanced proline and polyamines-induced ROS production in the AZs, thereby contributing to ETH production (Liao et al., 2016). Application of exogenous H_2O_2 is known to induce ETH production during cotton (Gossypium spp.) fiber development (Xiao et al., 2019). Suppression of the ROS scavenger *metallothionein2b* (*MT2b*) in rice (*Oryza sativa* L.) significantly enhanced both H_2O_2 and ETH signaling, revealing a positive feedback loop between the two (Steffens and Sauter, 2009). Contrarily, application of the ETH action inhibitor 1-methylcyclopropene (1-MCP) did not prevent H_2O_2-induced epidermal cell death. Additionally, the application of diphenyleneiodonium (DPI, a ROS inhibitor) caused suppression of ETH-induced abscission. Therefore, H_2O_2 is thought to act downstream of ETH in mediating abscission (Sakamoto et al., 2008).

Abscission of leaves, flowers, and fruits involves degradation of the primary cell wall or middle lamella pectin of AZ tissues by polygalacturonases and xyloglucan endotransglucosylases/hydrolases (Tucker et al., 1988; Cai-Zhong et al., 2008; Paz et al., 2017). A reduction in cell wall rigidity in AZ cells allows for their expansion, which provides the force for the abscission of the distal organ (Roberts et al., 1984). The rounded cells in the Arabidopsis (*Arabidopsis thaliana*) flower petal AZ could be observed in wild-type plants from positions 7 to 12, while a flattened fracture plane was observed at the same position in the AZs of abscission-defective mutant *ida* lines (Meir et al., 2019). During the separation of AZ cells, pronounced cell expansion was also reported in *Citrus sinensis* and in tomato pedicel AZ cells during ETH-induced abscission (Roberts et al., 1984; Butenko et al., 2003; Paz et al., 2017). Previous research has shown that cell expansion requires water influx (Braidwood et al., 2013). Waterlogging has been shown to enhance flower and young fruit abscission in bean crops (Najeeb et al., 2015). As waterlogging duration increased, cotton boll abscission was also shown to increase (Xiaosen et al., 2017). Hence, it can be inferred that water influx into the expanding cells of the AZ is a common phenomenon during abscission (Kumpf et al., 2013; Tranbarger et al., 2017).

Aquaporins (AQPs) physically interact with themselves or other AQP monomers to assemble into homo- and hetero-tetrameric units, which act as functional channels for water, urea, glycerol, H_2O_2, and CO_2 transport across cell membranes in all living cells (Bellati et al., 2010; Bienert et al., 2011). Plant AQPs can be classified into seven subfamilies based on their protein sequences: plasma membrane intrinsic proteins (PIPs), tonoplast intrinsic proteins (TIPs), NOD26-like intrinsic proteins (NIPs), X intrinsic proteins, hybrid intrinsic proteins, small basic intrinsic proteins, and GlpF-like intrinsic proteins (Wudick et al., 2009; Hacke et al., 2012). TIPs and PIPs show tissue- and cell type-specific expression patterns, and functional loss of specific AQPs leads to significant physiological alterations (Chaumont et al., 1998; Johansson et al., 2000). AtNIP1;1 shows a high transport capacity and modulates Arabidopsis sensitivity to H_2O_2 (Sadhukhan et al., 2017), whereas AtPIP1;4 aids in apoplastic H_2O_2 transport into the cytoplasm to enhance plant immunity and trigger cell death (Tian et al., 2016). Furthermore, expression of *AtPIP2;4*, *AtTIP1;1*, and *AtTIP1;2* in yeast is known to cause a significant decrease in survival rate under H_2O_2 treatment, indicating their roles in H_2O_2 transport (Jang et al., 2011; Bienert and Chaumont, 2014). The influx of H_2O_2, which results in a transient rise in cellular H_2O_2 levels, can trigger redox-sensitive transcription factors (TFs) and MAPK pathways to mediate cell hormone signaling and metabolism (Dimitrov and Frank, 2012; Niederhuth et al., 2013). In addition, there is considerable evidence that TIPs are involved in controlling cell expansion (Kumpf et al., 2013). *AtTIP1* from Arabidopsis and *ZmTIP1* from *Zea mays* are highly expressed in expanding cells, suggestive of a role for *TIP1* in water transport into vacuoles during cell expansion. In addition, overexpression of *BobTIP26* in *Nicotiana tabacum* L. cells is known to have significantly increased cell volume (Chaumont et al., 1998; Reisen et al., 2003; Beebo et al., 2009).

Water and H_2O_2 signaling are important for priming stem cell differentiation in both animals and plants (Day and Veal, 2011; Park et al., 2015; Zeng et al., 2017). Disruption of the undifferentiated cells in a meristem in order to initiate differentiation, such as expansion and separation of meristem-like AZ cells, requires molecular mechanisms to gate water and H_2O_2 transport; however, the underlying mechanisms are unknown (Djanaguiraman et al., 2004; Swaef and Steppe, 2010). Here, we tested the hypothesis that AQP-mediated H_2O_2 and H_2O transport is important for tomato flower pedicel abscission. Further, we described the characterization of the associated ETH and auxin regulatory frameworks in cell separation.

Results

The role of AQPs in tomato pedicel abscission

To test the role of water potential in tomato pedicel abscission, the rate of abscission under double distilled water, 1/4 artificial xylem sap (AXS), 1/2 AXS, and AXS solutions were compared. In double-distilled water, pedicel explants reached 100% abscission in 32 h. As the water potential decreased, the explant abscission decreased: 1/4 AXS, 1/2 AXS, and AXS treatments reached 78%, 76%, and 65% abscission, respectively, in 32 h (Figure 1A). Since the flow of water and other small molecules across cell membranes is largely modulated by AQPs, we also used two different specific AQP inhibitors, $HgCl_2$ and phloretin, to treat pedicel explants. Both treatments significantly inhibited osmotic stress-induced abscission (Figure 1, B and C), and treatment with 1-MCP had the same effect (Figure 1D).

SlTIP1;1 is the most abundantly expressed AQP in the AZ

Next, we aimed to identify specifically and highly expressed AQP members in the tomato flower pedicel AZ during abscission. The putative size of tomato PIPs and TIPs range from 25 to 32 kDa; hence, proteins of this size range were purified from the AZ, based on SDS–PAGE, and analyzed by mass spectrometry. Mass spectra derived from analyses of all the fractions were compared to sequences in the tomato AQP database, and peptides were identified according to the intensity-based absolute quantification method. The spectral counts and statistical analysis of the mass spectrometry results indicated that a total of eight AQP proteins were identified at 0, 16, and 32 h: SlPIP1;3 (19.91%, 22.32%, and 20.98%), SlPIP1;5 (23.50%, 28.35%, and 26.52%), SlPIP1;7 (0.31%, 0.19%, and 0.26%), SlPIP2;4 (3.00%, 1.72%, and 2.52%), SlPIP2;5 (1.85%, 0.93%, and 1.55%), *SlTIP1;1* (50.17%, 45.50%, and 47.20%), SlTIP4;1 (0.95%, 0.72%, and 0.61%), and SlNIP5;1 (0.31%, 0.27%, and 0.36%; Figure 2; Supplemental Table S1). We further focused on the role of *SlTIP*1;1, which had the highest accumulation among the various AQPs in the AZ.

SlTIP1;1 has AZ-specific expression patterns during abscission

The expression patterns of *SlTIP1;1* were further analyzed during pedicel abscission, using non-AZ (NAZ)- and 1-MCP-treated AZs as nonabscising controls. The expression of *SlTIP1;1* in the AZ showed a continuous increase and reached a peak at 16 h during abscission. *SlTIP1;1* increase was highly AZ-specific and was inhibited by 1-MCP treatment (Figure 3A). In situ hybridization revealed that *SlTIP1;1* was predominantly expressed in the AZ. Its expression significantly increased in the AZ with abscission progression and positive signals were highly abundant in the vascular bundle at 16 h, consistent with the fact that abscission often begins near vascular bundles (Tabuchi et al., 2001; Figure 3B). To determine whether the high mRNA expression resulted in abundant accumulation of the corresponding protein, different abscission-stage AZ samples were subjected to western blot analysis using 40s ribosomal protein as a control since its expression is stable during abscission (Zhang et al., 2015). The *SlTIP1;1* protein concentrations reached a peak at 16 h in the induced abscission sample, while treatment with 1-MCP suppressed the increase of *SlTIP1;1* protein, maintaining it at a lower level (Figure 3, C and D).

Subcellular localization of *SlTIP1;1*

We next introduced *SlTIP1;1*-green fluorescent protein (GFP) fusion proteins into Arabidopsis protoplasts. Protoplasts transformed with only the p35S:GFP vector exhibited fluorescence throughout the cells. Heterologously expressed *SlTIP1;1*-GFP signal showed co-localization with FM4-64 and labeled the plasma membrane and vacuolar membrane in the plants (Rigal et al., 2015); a weak *SlTIP1;1*-GFP signal was observed on the plasma membrane, while a strong accumulation was observed in the vacuolar membrane (Figure 4A).

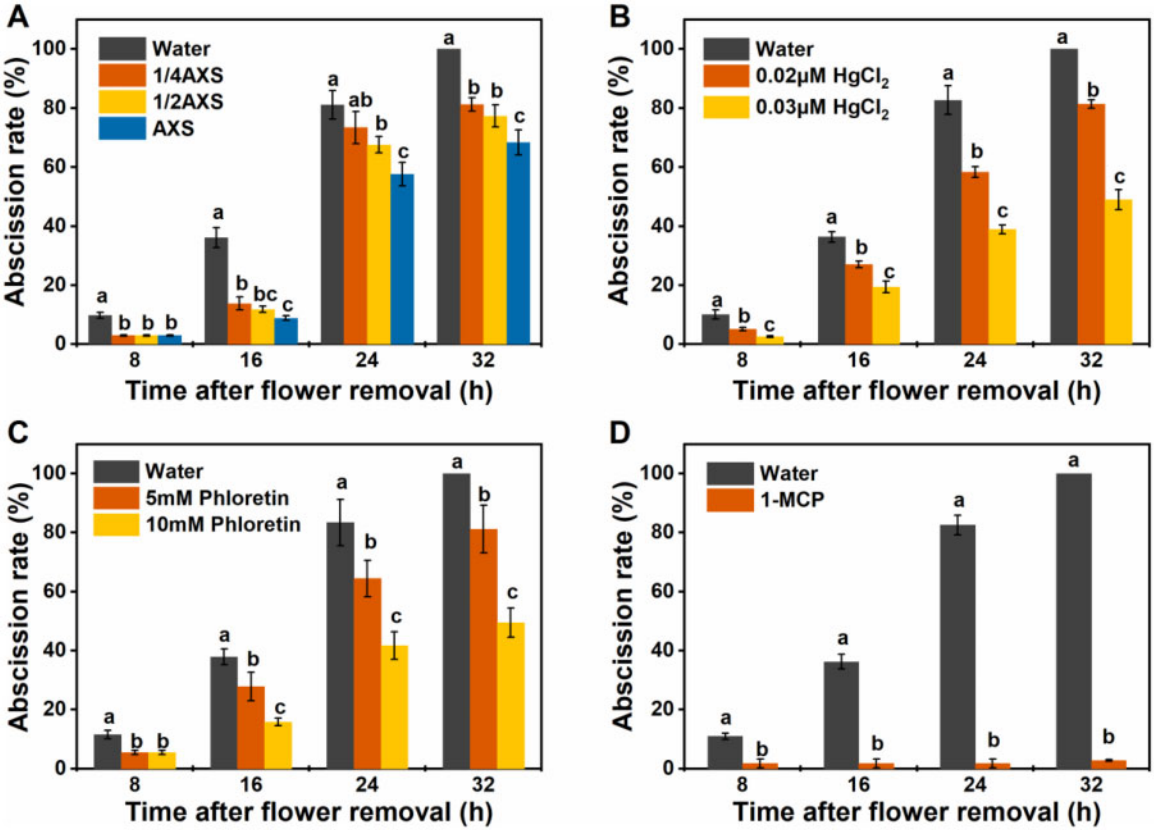

Figure 1 ETH and AQPs are required for osmotic stress induced abscission. A, The effect of different osmotic stresses on pedicel abscission. AQP inhibitors, $HgCl_2$ (B), and phloretin (C), suppressed osmotic stress induced-abscission. D, The effect of 1-MCP pretreatment on osmotic stress-induced abscission. Values are presented as means of measurements from three independent experiments ±SD, with 50 samples per replicate. Different lowercase letters signify significant differences between means (Student's *t* test, $P < 0.05$). AXS, artificial xylem sap; 1-MCP, 1-methylcyclopropene.

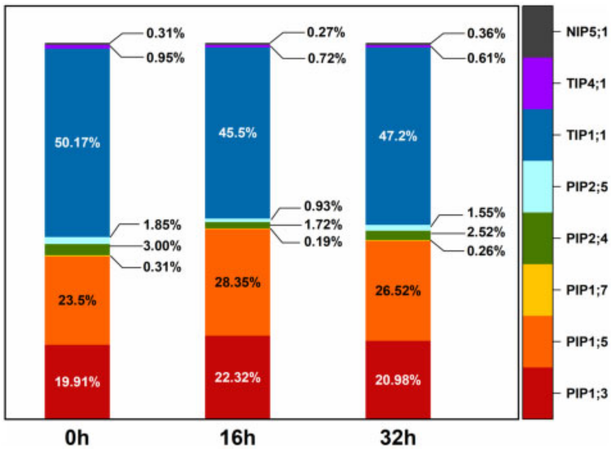

Figure 2 AQP protein accumulation in pedicel AZ during abscission. Summary of the mass spectrometry determined absolute values of tomato AQP homologs from 25 to 32-kDa AZ plasma membrane protein fraction sampled at 0, 16, and 32 h. Values are the means of three replicates ± SD.

To verify this result, we also used anti-*SlTIP1;1* antibody to examine their subcellular location in AZ cells. *SlTIP1;1* was localized in the central vacuole, small vacuole tonoplast, and plasma membrane (Figure 4B).

SlTIP1;1 mediated tomato pedicel abscission

To further investigate the contribution of *SlTIP1;1* to tomato pedicel abscission, we created *SlTIP1;1* overexpression lines and used clustered regularly interspaced short palindromic repeat (CRISPR)/Cas9 technology to obtain *SlTIP1;1* knockout (KO) lines. After PCR screening and measurement of *SlTIP1;1* mRNA levels, we obtained six independent *35S:SlTIP1;1* lines; among them, five showed a significant increase in *SlTIP1;1* expression in the AZ (Supplemental Figure S2). The KO results were verified by sequencing the PCR products amplified using *SlTIP1;1*-specific primers. Three transgenic lines were confirmed to be homozygous based on sequencing of the PCR products (Supplemental Figure S3)

Abscission assays indicated that wild type reached 75% abscission at 24 h and 100% abscission at 32 h. Overexpression of *SlTIP1;1* significantly accelerated the abscission rate, such that 100% abscission was reached at 24 h, whereas KO of *SlTIP1;1* significantly delayed abscission, with 35 and 46% abscission rates at 24 h and 32 h, respectively (Figure 5A). Using ROS scavengers, DPI significantly depressed abscission in the wild-type, *35S:SlTIP1;1*, and *CR-sltip1;1* lines; there was no significant difference in abscission among wild-type, *35S:SlTIP1;1*, and *CR-sltip1;1* before 24 h (Figure 5B). We further assayed the response of wild-type and transgenic lines

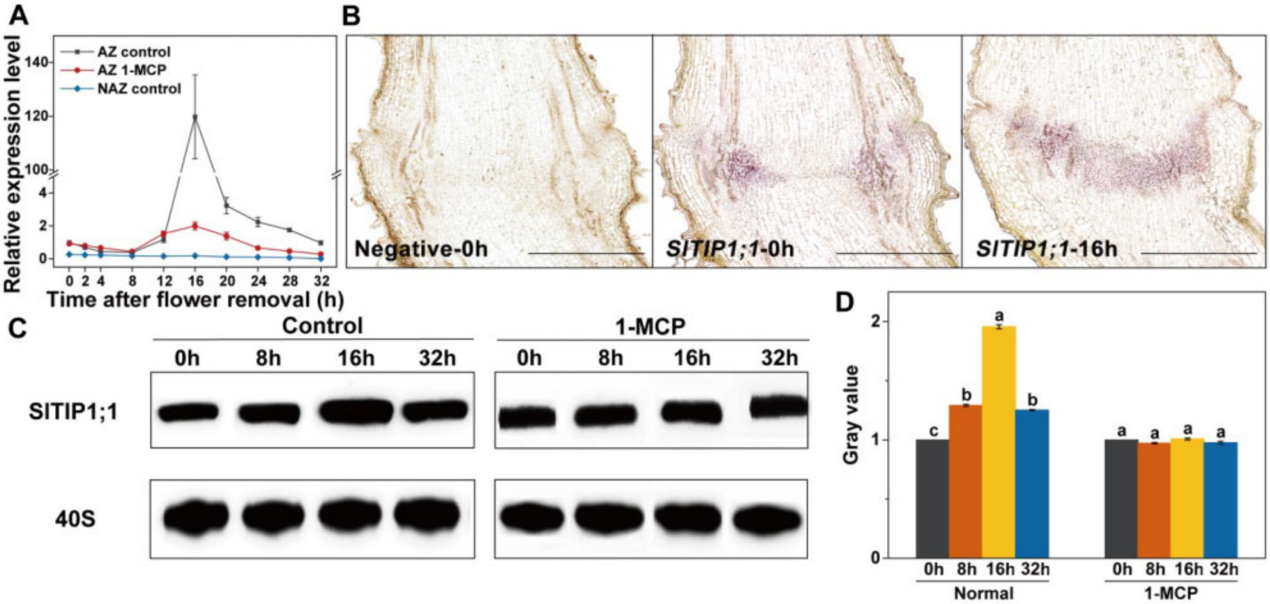

Figure 3 RT-qPCR, in situ hybridization, and Western blot analysis of *SlTIP1;1* abscission-related expression. A, RT-qPCR analysis of *SlTIP1;1* expression during abscission. Values are the means of three replicates ±SD. B, Those built of multiple images in situ hybridization revealed that *SlTIP1;1* is preferentially expressed in the AZ during abscission. A *SlTIP1;1* sense probe was used as a negative control; 0 and 16 h pedicels showed a signal for *SlTIP1;1*. Scale bars = 500 µm. C, The accumulation of *SlTIP1;1* in AZ during flower removal-induced abscission (control) and without abscission induction (flower removal with 1-MCP treatment) detected by Western blot analysis using specific antibodies against *SlTIP1;1* and the marker protein 40 S. D, Quantification of *SlTIP1;1* in the AZ during abscission. Values are the means of three replicates ±SD, with three biological replicates. Different lowercase letters signify significant differences between means (Student's *t* test, $P < 0.05$). 1-MCP, 1-methylcyclopropene.

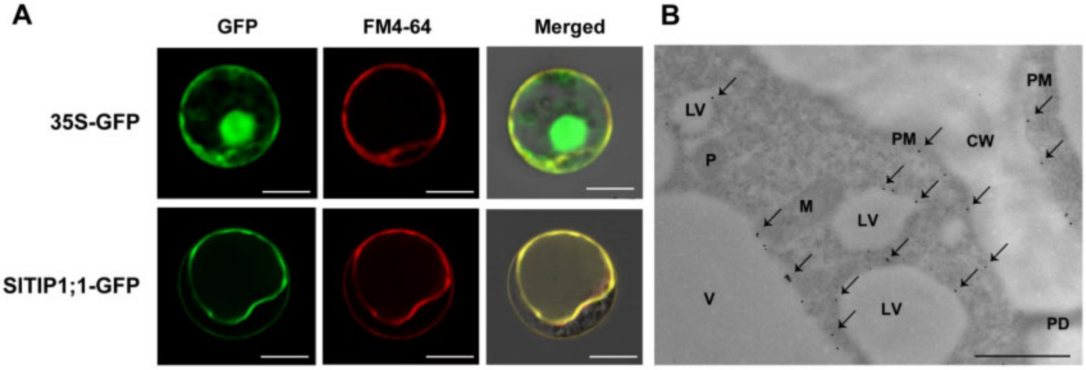

Figure 4 Subcellular localization of *SlTIP1;1* determined in *A. thaliana* mesophyll protoplasts and tomato pedicel AZs. A, Protoplasts stained with FM4-64 and transiently expressing GFP and *SlTIP1;1*-GFP. The sizes of the *A. thaliana* mesophyll protoplasts ranged from 30 to 50 µm. B, Sections incubated with 1/50 diluted anti-*SlTIP1;1* and treated with GAR-IgG-15 nm gold secondary antibody. Immunolabeling of the *SlTIP1;1* protein in the tonoplast and lytic vacuoles, with a specific signal also detected in the plasma membrane (black arrow). PM, plasma membrane; P, plastid; PD, plasmodesmata; M, mitochondria; V, vacuole; LV, lytic vacuole; CW, cell wall. Scale bar = 10 µm.

to H_2O_2 treatment. In contrast to wild-type, which had 70% abscission at 16 h and 100% abscission at 24 h, the *35S:SlTIP1;1* line showed accelerated effects and reached 90% abscission at 16 h, while the *CR-sltip1;1* line had retarded abscission and reached only 41% abscission at 24 h (Figure 5C). Under ETH treatment, the wild-type line reached 72% abscission at 16 h and complete abscission at 24 h; in contrast, the *35S:SlTIP1;1* line reached 100% abscission at 16 h while the *CR-sltip1;1* line reached 48% abscission at 24 h (Figure 5D).

SlTIP1;1 affects apoplastic and cytoplasmic H_2O_2 accumulation during abscission

To investigate whether *SlTIP1;1* affects H_2O_2 levels in AZ cells, we employed the H_2O_2 probes Amplex ultra red (AUR) and Amplex red (AR) to quantify the apoplastic and cytoplasmic H_2O_2 concentrations (Tian et al., 2016), respectively, in the AZ of wild-type, *35S:SlTIP1;1* and *CR-sltip1;1* lines during abscission (Figure 6, A and B). There was no difference in the apoplastic and cytoplasmic H_2O_2 concentrations (AUR and AR signal) among wild-type, *35S:SlTIP1;1*,

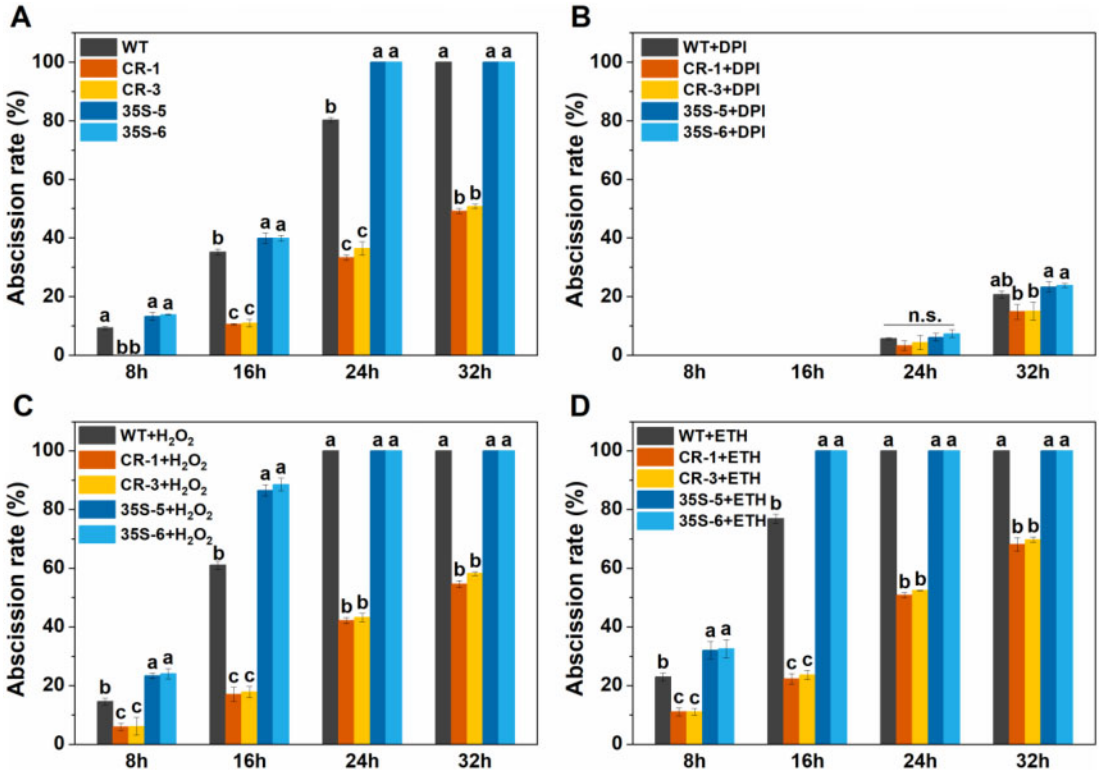

Figure 5 Pedicel abscission assay in wild-type, *35S:SlTIP1;1*, and *CRsltip1;1* lines. A, Abscission of wild-type (WT), *35S:SlTIP1;1* (35S-5, 35S-6), and *CRsltip1;1* (CR-1, CR-3) pedicel explants incubated in water. B, The effect of ROS scavengers DPI on abscission of WT, *35S:SlTIP1;1* (35S-5, 35S-6), and *CRsltip1;1* (CR-1, CR-3) lines. C, Abscission of WT, *35S:SlTIP1;1* (35S-5, 35S-6), and *CRsltip1;1* (CR-1, CR-3) lines treated with 0.5 mM H_2O_2. D, Abscission of WT, *35S:SlTIP1;1* (35S-5, 35S-6), and *CRsltip1;1* (CR-1, CR-3) lines treated with 20 μL L^{-1} ETH. Values are the means of three replicates ± SD, with 20 samples per replicate. Different lowercase letters represent significant differences between means (Student's *t* test, $P < 0.05$).

and *CR-sltip1;1* AZs before flower removal. After flower removal, both apoplastic and cytoplasmic H_2O_2 concentrations increased significantly in the wild-type AZ. Notably, these increases were very rapid, with significantly higher apoplastic and cytoplasmic H_2O_2 concentrations found in the wild-type AZ at 4 h than at 0 h. Compared to wild-type, *SlTIP1;1* resulted in significantly reduced apoplastic and cytoplasmic H_2O_2 levels, i.e. 58% reduction in apoplastic H_2O_2 quantities and 72% reduction in cytoplasmic H_2O_2 quantities at 16 h. Overexpression of *SlTIP1;1* resulted in significantly increased apoplastic and cytoplasmic H_2O_2 levels, i.e. a 12% increase in apoplastic H_2O_2 quantities and a 20% increase in cytoplasmic H_2O_2 quantities at 16 h. To further explore the role of *SlTIP1;1* in apoplastic and cytoplasmic H_2O_2 concentrations, we incubated wild-type, *35S:SlTIP1;1*, and *CR-sltip1;1* explants in H_2O_2. H_2O_2 treatment enhanced apoplastic and cytoplasmic H_2O_2 concentrations in the AZ of wild-type and *35S:SlTIP1;1* lines; in the AZ of *CR-sltip1;1*, contrarily, it enhanced apoplastic H_2O_2 concentration but affected cytoplasmic H_2O_2 concentration to a lesser degree (Figure 6, C and D).

De novo expression of *SlTIP1;1* and H_2O_2 translocation assay in yeast

To provide additional evidence of the role of *SlTIP1;1* in H_2O_2 transport, the yeast wild-type strain, BY4741, and the KO strain, *yca*1, were transformed with recombinant vectors expressing *SlTIP1;1* (Figure 7). The *yca1* KO line is defective in apoptosis due to the loss of function of the yeast caspase-like protein *Yor197w*, resulting in partial tolerance to H_2O_2 (Liang et al., 2008). The yeast strains were also transformed with a vector expressing *AtPIP2;4* as a positive control because it is known to significantly increase yeast sensitivity to H_2O_2 (Hooijmaijers et al., 2012). The yeast cells transformed with *SlTIP1;1* were more sensitive to H_2O_2 than the control strains carrying the empty vector; BY4741 growth was severely affected when exposed to 1.5 mM and 2 mM H_2O_2, and *yca1* growth was similarly affected upon exposure to 2 mM and 2.5 mM H_2O_2, confirming the role of *SlTIP1;1* in facilitating H_2O_2 translocation in yeast.

SlTIP1;1 is involved in cytoplasmic H_2O_2 transport in AZ protoplasts

Next, the H_2O_2 transport of *SlTIP1;1* in tomato was investigated by measuring intracellular H_2O_2 levels in wild-type AZ protoplasts treated with 0 or 3 mM H_2O_2 (Figure 8). In wild-type protoplasts, H_2O_2 treatment resulted in a 1.5-fold increase in intracellular H_2O_2 levels after 12 min incubation. In *35S:SlTIP1;1* protoplasts, H_2O_2 incubation led to a two-fold increase in intracellular H_2O_2 levels. Protoplasts from the *CR-sltip1;1* line showed only a 0.5-fold increase in

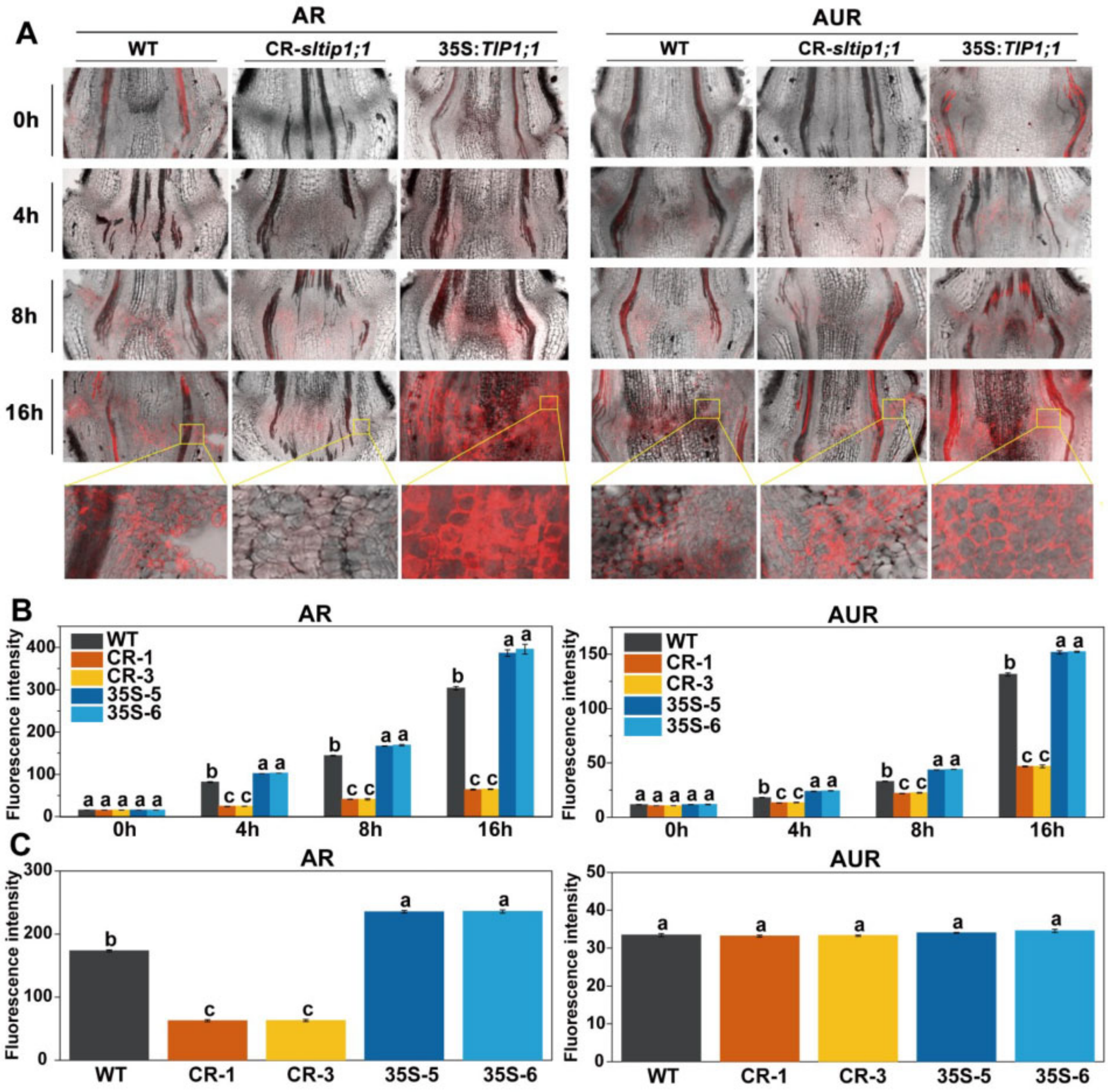

Figure 6 *SlTIP1;1*-mediated cytoplasmic H_2O_2 accumulation during abscission. A, Imaging of AR- or AUR-stained WT, 35S-6, and CR-1 AZs showing H_2O_2 levels. B, Alteration of apoplast and cytoplasmic H_2O_2 concentrations in WT, *35S:SlTIP1;1* (35S-5, 35S-6), and *CRsltip1;1* (CR-1, CR-3) AZ cells. C, The effect of H_2O_2 on cytoplasmic H_2O_2 concentrations in WT, *35S:SlTIP1;1* (35S-5, 35S-6), and *CRsltip1;1* (CR-1, CR-3) AZ cells. Three independent experiments were performed. Data are expressed as mean ± SD (*n* = 10 in each group). Different lowercase letters represent significant differences between means (Student's *t* test, $P < 0.05$).

intracellular H_2O_2, suggesting significantly retarded H_2O_2 transport in the *CR-sltip1;1* line.

SlTIP1;1 links auxin signaling and ETH production during abscission

The *CR-sltip1;1* line showed significantly delayed H_2O_2-induced and ETH-induced abscission (Figure 5, C and D). Since previous research indicated that downregulation of the auxin signal is required for abscission (Sakamoto et al., 2008), auxins delay the onset of early stages of abscission but promote the later stages, and the first 4 h after auxin depletion are assumed to be early events of abscission (Meir et al., 2010). We also investigated the AZ cellular auxin signal by analyzing a *DR5::VENUS* signal in wild-type and *CR-sltip1;1* lines during normal and H_2O_2- or ETH-induced abscission (Figure 9). The *DR5::VENUS* promoter is directly bound by multiple ARFs, and the VENUS signal therefore reflects the combined activity of all cellular ARFs. There was no difference in auxin signals between the *CR-sltip1;1* and wild-type lines at 0 h. After auxin depletion (flower removal), the *DR5::VENUS* signal was significantly decreased in the AZ of wild-type at 4 h. Moreover, H_2O_2 and ETH treatment further reduced the wild-type AZ *DR5::VENUS* signal (Figure 9). Notably, *RBOH1* is upregulated immediately after flower removal, i.e. within 2 h (Bar-Dror et al., 2011), and, in this study, apoplastic and cytoplasmic H_2O_2 concentrations were found to be increased in the wild-type (Figure 6). *CR-sltip1;1* AZ cells showed higher cellular auxin signals at 4 h after flower removal than the wild-type, even under H_2O_2 and ETH treatment, indicating that the inhibition of cytoplasmic H_2O_2 elevation in the *CR-sltip1;1* AZ resulted in a higher *DR5::VENUS* signal during abscission. Moreover, *CR-sltip1;1* was more sensitive to auxin-inhibited abscission (Figure 9C), indicating the role of *SlTIP1;1* in mediating auxin homeostasis by altering cytoplasmic H_2O_2 homeostasis.

ETH production of wild-type AZ explants showed an increasing trend and reached a peak at 8 h and then decreased during abscission. Compared to the wild-type, overexpression of *SlTIP1;1* significantly enhanced ETH production, while *CR-sltip1;1* explants had significantly reduced ETH production. Compared to the control (Figure 10A), ROS scavenger DPI treatment depressed ETH production in wild-type, *35S:SlTIP1;1*, and *CR-sltip1;1* AZ explants, and no significant difference was found among these lines in this regard (Figure 10B). Under H_2O_2 treatment, compared to wild-type AZ explants, *35S:SlTIP1;1* showed higher ETH production while *CR-sltip1;1* showed lower ETH production (Figure 10C).

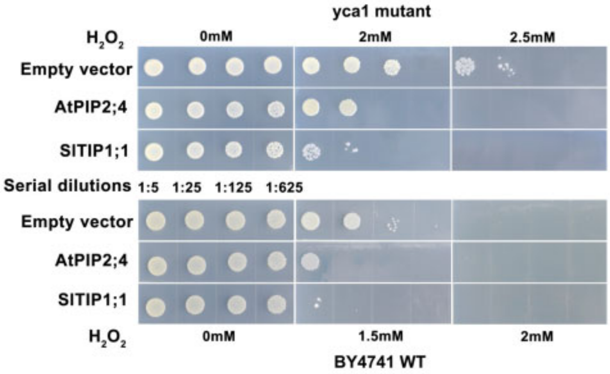

Figure 7 *SlTIP1;1* mediates H_2O_2 transport in yeast. The *S. cerevisiae* strains used in the H_2O_2 transport assays were WT (BY4741) and the *yca1* mutant. WT and *yca1* strains expressing *AtPIP2;4* and *SlTIP1;1* were used in a growth assay on solid medium. Cultures harboring empty *pYES2.0* vector were used as a negative control, and *pYES2.0-AtPIP2;4* as a positive control. Serial five-fold dilutions of liquid yeast nitrogen base (YNB) cultures were spotted on solid YNB medium containing 0, 1.5, 2, or 2.5 mM H_2O_2 and photographed after 4 d. Three independent experiments were performed.

SlERF52 directly binds to *SlTIP1;1* promoters and activates its transcription

SlTIP1;1 expression increased after flower removal and peaked at 16 h, this increased expression was completely inhibited by 1-MCP treatment, suggesting that it is regulated by ETH. During abscission, ethylene response factor 52 (*SlERF52*) is known to play a pivotal role in pedicel AZ transcriptional regulation. Downregulation of *SlERF52* has been reported to cause suppressed cell expansion and delayed abscission, but the direct SlERF52 target genes are still unknown (Nakano et al., 2014). The *SlERF52* silencing lines showed significantly suppressed expression of *SlTIP1;1* (Figure 11A). We next investigated the binding of SlERF52 to the *SlTIP1;1* promoter using a yeast one hybrid (Y1H) assay (Figure 11B). Further analysis showed that SlERF52 bound to fragments containing the dehydration-responsive element (DRE; CCGAC) motif (*SlTIP1;1*: −296 to −292 bp from the start ATG). To confirm this interaction, an electrophoretic mobility shift assay (EMSA) was performed with the SlERF52 protein and fragments of the biotin-labeled *SlTIP1;1* promoter containing the DRE motif. When an unlabeled probe with a mutated DRE element was used as the competitor, the binding of SlERF52 to the *SlTIP1;1* promoter fragments was not altered, suggesting that SlERF52 indeed binds to the *SlTIP1;1* promoter (Figure 11C). We then assayed *SlTIP1;1*

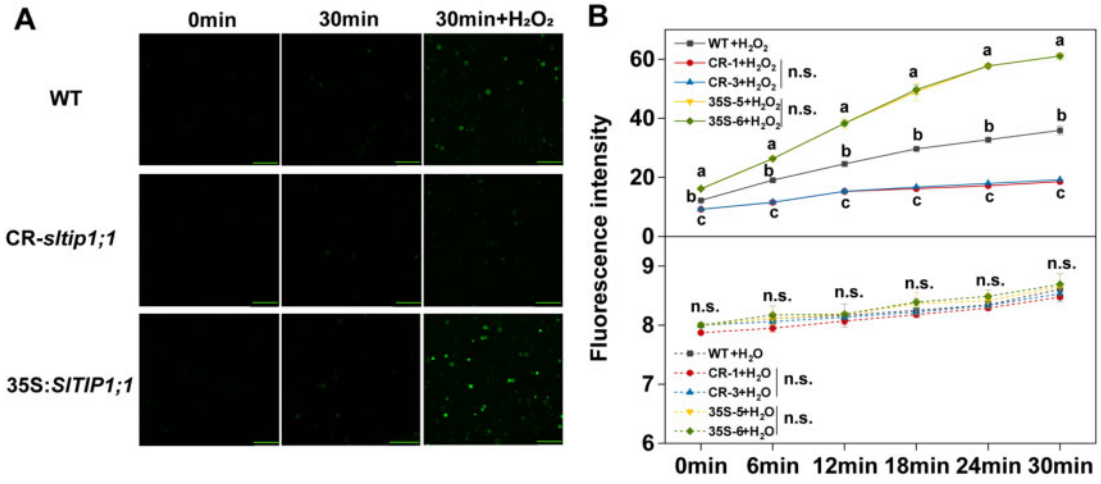

Figure 8 The roles of *SlTIP1;1* on H_2O_2 transport in the pedicel AZ. A, Fluorescence imaging after addition of 5 μM H2DCFDA dye to WT, 35S-6, and CR-1 AZ cells treated with or without 3 mM H_2O_2. Alteration of H2DCFDA fluorescence intensity in WT, *35S:SlTIP1;1*(35S-5, 35S-6), and *CRsltip1;1*(CR-1, CR-3) AZ cells with or without 3 mM H_2O_2 (B) (mean ± SD; *n* = 20). Three independent experiments were performed. Different lowercase letters represent significant differences in means (Student's *t* test, $P < 0.05$). Scale bars = 150 μm.

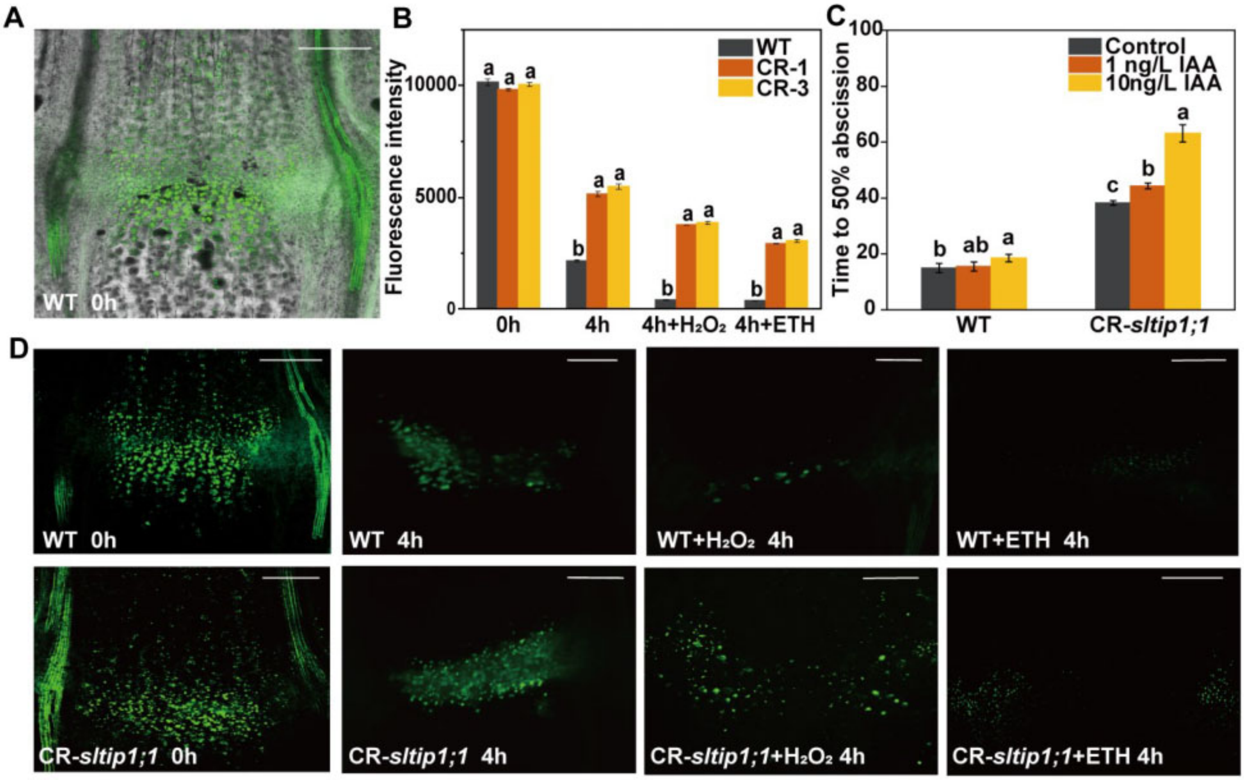

Figure 9 A high auxin signal is observed in *CRsltip1;1* lines compared to WT. A and D, *DR5::VENUS* signal in WT and CR-1 AZs at 0 h after flower removal. The *DR5::VENUS* signal in WT and CR-1 AZs treated with H_2O_2 at 16 h after flower removal. *DR5::VENUS* signal in WT and CR-1 AZs treated with ETH at 16 h after flower removal. Scale bars = 150 µm. B, Alteration of fluorescence intensity in WT and *CRsltip1;1*(CR-1, CR-3) AZ cells. C, Auxin (IAA) inhibited abscission assay in WT and *CRsltip1;1*(CR-1, CR-3). The time to 50% abscission rates were determined after WT and *CRsltip1;1*(CR-1, CR-3) pedicels were incubated with different concentrations of auxin. Three independent experiments were performed. Data are expressed as mean ± SD ($n = 30$). Different lowercase letters represent significant differences between means (Student's *t* test, $P < 0.05$).

promoter regulation by SlERF52 using a glucuronidase (GUS) transactivation assay in *Nicotiana benthamiana* leaves. We co-transformed *35S:SlERF52* and *ProSlTIP1;1:GUS*. SlERF52 significantly increased *SlTIP1;1* promoter activity, while the activity of the mutant *SlTIP1;1* promoter remained unchanged (Figure 11D). These results suggest that ETH induces SlERF52 to activate *SlTIP1;1* expression, and that *SlTIP1;1* functions downstream of the ETH signal to accelerate abscission.

Role of *SlTIP1;1* in late events of abscission via water transport activity

We hypothesized that *SlTIP1;1* might also mediate water transport into AZ cells to drive the abscission process. To test this, we examined its activity by heterologous expression in *Xenopus laevis* oocytes (Figure 12A). In a hypotonic solution, oocytes expressing *SlTIP1;1* expanded rapidly, in contrast to those under the control treatment (distilled water). The P_f values of oocytes expressing *SlTIP1;1* were approximately 9.7-fold higher than those of the controls. We next determined the P_f values of protoplasts from the wild-type, S:*SlTIP1;1*, and *CR-sltip1;1* lines (Figure 12B). Compared to the wild-type AZ (P_f 26.4), the P_f of *CR-sltip1;1* AZ cells decreased to 11.8, while the P_f of *35S:SlTIP1;1* AZ cells increased to 31.3. Moreover, after DPI treatment for 32 h, *35S:SlTIP1;1* showed slightly higher abscission than the wild-type, and significantly higher abscission than the *CR-sltip1;1* line (Figure 5B).

Discussion

SlTIP1;1 is highly expressed in the pedicel AZ during abscission and is located in both the tonoplast and plasma membrane

Abscission is a complex physiological process, and includes an associated increase in cytosolic pH, ROS production, and starch degradation, which facilitate water influx; further, this process is thought to be accelerated by ETH (Lloyd et al., 1989; Lers et al., 2006; Bar-Dror et al., 2011; Caiqin et al., 2015; Srivignesh et al., 2015; Menghan, 2018). Since AQP inhibitors suppress abscission, AQPs are assumed to be required for this process (Figure 1). However, the specific AQP genes involved in abscission are still unknown. Here, we identified *SlTIP1;1* as the most abundant AQP. Heterologous expression of *SlTIP1;1* in Arabidopsis protoplasts showed that EGFP-*SlTIP1;1* was detected in the central vacuole tonoplast and plasma membrane, and in situ immunolocalization of *SlTIP1;1* confirmed the presence of *SlTIP1;1* in the vacuoles and the plasma membrane (Figures 2–4). AtTIP1;2,

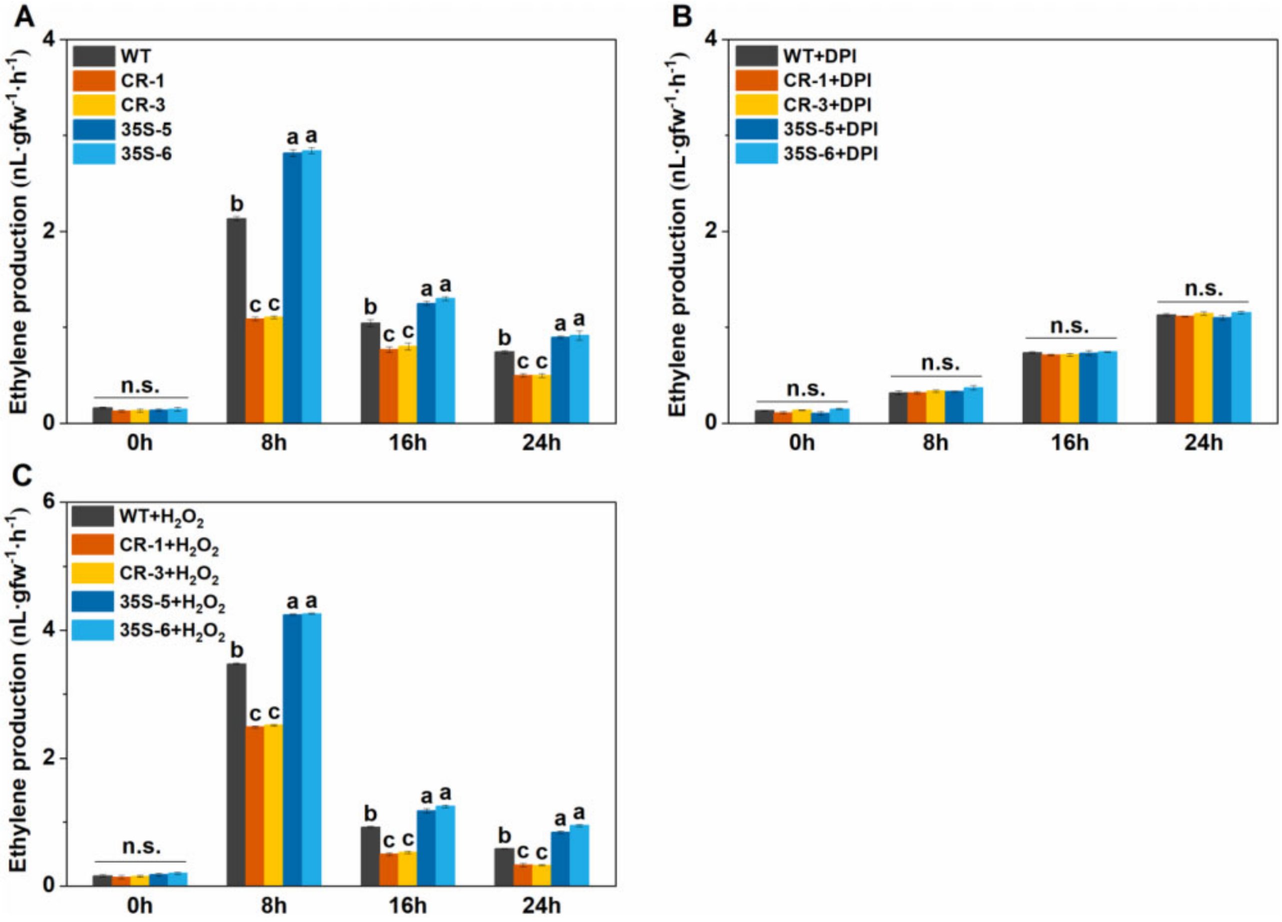

Figure 10 *SlTIP1;1*-mediated ETH production during abscission. A, ETH production in WT, *35S:SlTIP1;1*(35S-5, 35S-6), and *CRsltip1;1*(CR-1, CR-3) AZ explants at 0 and 16 h after flower removal. B, The effect of the ROS scavenger DPI on WT, *35S:SlTIP1;1*(35S-5, 35S-6), and *CRsltip1;1*(CR-1, CR-3) AZ explants ETH production. C, The effect of H_2O_2 on the ETH production of WT, *35S:SlTIP1;1*(35S-5, 35S-6), and *CRsltip1;1*(CR-1, CR-3) AZ explants. Three independent experiments were performed. Data are expressed as mean ± SD. Different lowercase letters represent significant differences between means (Student's *t* test, $P < 0.05$).

AtTIP2;1, AtTIP3.1, AtTIP3.2, and AtTIP4;1 have been reported to be present in the plasma membrane, suggesting that TIPs also have a function there (Luu and Maurel, 2013). The predominant distribution of *SlTIP1;1* in the tonoplast and plasma membrane suggests possible functions in mediating influx or efflux to the cytoplasm and vacuoles of small molecules during abscission. AtTIP1;1 from Arabidopsis and CmTIP1;1 and CmTIP1;2 from *Cucumis melo* are also found to be extensively expressed during abscission, suggesting that TIP function in abscission is conserved across species (Corbacho et al., 2013; Niederhuth et al., 2013). In this study, *SlPIP*1;3 and *SlPIP*1;5 also showed high accumulation in the AZ during abscission; however, further studies are required to elucidate their roles in abscission.

Role of *SlTIP1;1* in mediating cytoplasmic H_2O_2

Extracellular ROS scavengers and RBOH inhibitors show a powerful effect on abscission, indicating that continuous extracellular H_2O_2 produced by NADPH oxidase is a major resource for inducing abscission (Addicott, 1982; Sakamoto et al., 2008). H_2O_2 is a stable form of ROS and a common substrate for TIPs; however, the role of H_2O_2 transported through AQPs in abscission is unclear. Cytoplasmic H_2O_2 plays a vital role in mediating development and response to environmental stimuli. The H_2O_2-transport role of *AtPIP*1;4 is essential for the cytoplasmic import of apoplastic H_2O_2 in order to trigger immune responses induced by bacterial pathogens and two typical PAMPs (Tian et al., 2016). Overexpression of *TsTIP*1;2 enhances H_2O_2 influx into the cytoplasm of yeast cells and inhibits cell growth (Schüssler et al., 2010; Wang et al., 2014). We observed that, compared to wild-type, a *SlTIP1;1* KO line had lower cytoplasmic H_2O_2 concentrations in the AZ cells, while overexpression lines showed enhanced H_2O_2 cytoplasmic accumulation during abscission (Figure 6). The yeast and protoplast assays further suggested that *SlTIP1;1* was involved in the transport of H_2O_2 into cells (Figures 7 and 8). Furthermore, KO lines were insensitive to H_2O_2- induced abscission while *SlTIP1;1* overexpression lines were more sensitive to H_2O_2 treatment than the wild-type, suggesting that *SlTIP1;1* is an essential element for H_2O_2 signal-triggered abscission (Figure 5). Notably, H_2O_2 treatment showed no difference in apoplast

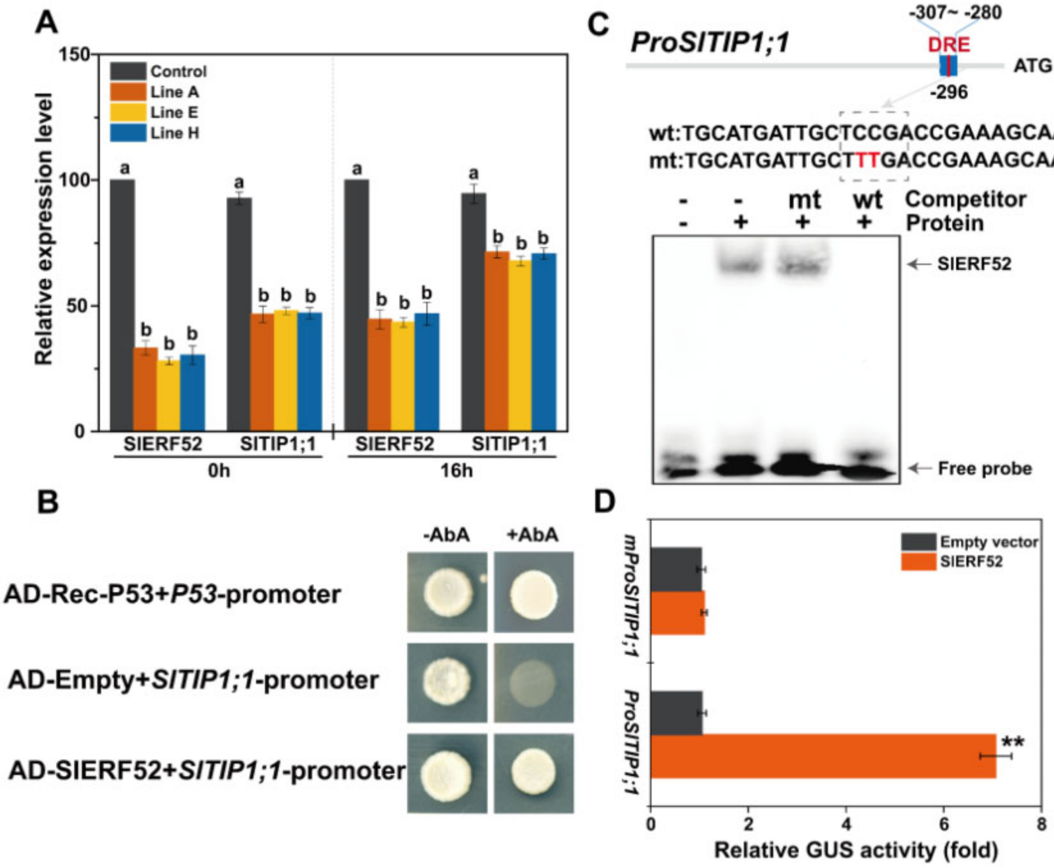

Figure 11 SlERF52 positively regulates *SlTIP1;1* transcription. A, The expression of *SlTIP1;1* in the AZ of control (Col; infected with TRV vectors) and *SlERF52* silenced (infected with TRV vectors containing fragments of the *SlTIP1;1* gene) lines (randomly select three lines, Line A, Line E, and Line H). Values are the means of three replicates ± SD, with 15 samples per replicate. Different lowercase letters represent significant differences between means (Student's *t* test, $P < 0.05$). B, Y1H assay revealed that *SlERF52* directly binds to the promoter fragment of *SlTIP1;1* containing the DRE. Co-transformed AD-*Rec-P53* and P53-promoter fragments in Y1HGold were used as positive controls. Empty vector and *SlTIP1;1* promoter fragments were used as negative controls. C, EMSA results revealing that SlERF52 binds to the ETH-responsive elements of the *SlTIP1;1* promoter. His-tagged SlERF52 was purified and used for analysis. The probes were biotin-labeled AQP promoter fragments containing ETH-responsive elements. The probe sequences for *SlTIP1;1* are shown and red letters represent the DRE. The mutated bases in the probe are represented by red letters. wt, intact DRE element; mt, probe with mutated DRE element. The unlabeled probes were added in 1,000-fold excess as competitors. The bands and free probes are annotated by arrowheads. D, β-GUS activity analysis indicating that SlERF52 induces the expression of *SlTIP1;1*. The reporter vectors containing the *SlTIP1;1* promoter or mutant, together with the SlERF52 effector vector, were co-expressed in tobacco leaves and GUS activities examined. Three independent experiments were performed. Data are expressed as mean ± SD. Asterisks represent significant differences in a multiple comparison, as calculated using a Student's *t* test. (**$P < 0.01$). AbA, Aureobasidin A.

H_2O_2 concentration among wild-type, KO, and overexpression lines, but a lower cytoplasmic H_2O_2 concentration in the KO line and higher H_2O_2 concentration in the *SlTIP1;1* overexpression line indicated a role for *SlTIP1;1* in transport but not the removal of H_2O_2 (Figure 6C).

Loss of function of *AtTIP1;1* and *AtTIP1;2* showed a weak ROS stress phenotype (Schüssler et al., 2010). TIPs are often deemed ROS scavengers, since vacuoles rich in flavonoids, ascorbate, and peroxidases usually seem to be a detoxification pool for stress-induced ROS (Yamasaki et al., 1997; Schüssler et al., 2010; Agati et al., 2012). However, H_2O_2 accumulation has also been detected in pea (*Pisum sativum*) leaf vacuolar membranes under Cd^{2+} stress and cotton glandular tonoplasts during program cell death procession (Wang et al., 2016; Zhang et al., 2017). These results imply a different H_2O_2 detoxification capacity system in different plant organs. This hypothesis is also supported by the increased oxidative stress and lower antioxidant activity observed in the AZ during tomato flower and fruit abscission (Djanaguiraman et al., 2004). A similar phenomenon was also observed in ETH-induced citrus leaf abscission, where the expression of antioxidant genes (both nonenzymatic and enzymatic) was much higher in nonabscising tissue than in the laminar AZ (Merelo et al., 2017). Hence, *SlTIP1;1* may facilitate H_2O_2 transport into the cytoplasm if the antioxidant system is not able to scavenge ROS efficiently, leading to excessive accumulation of H_2O_2 in the cytoplasm of AZ cells.

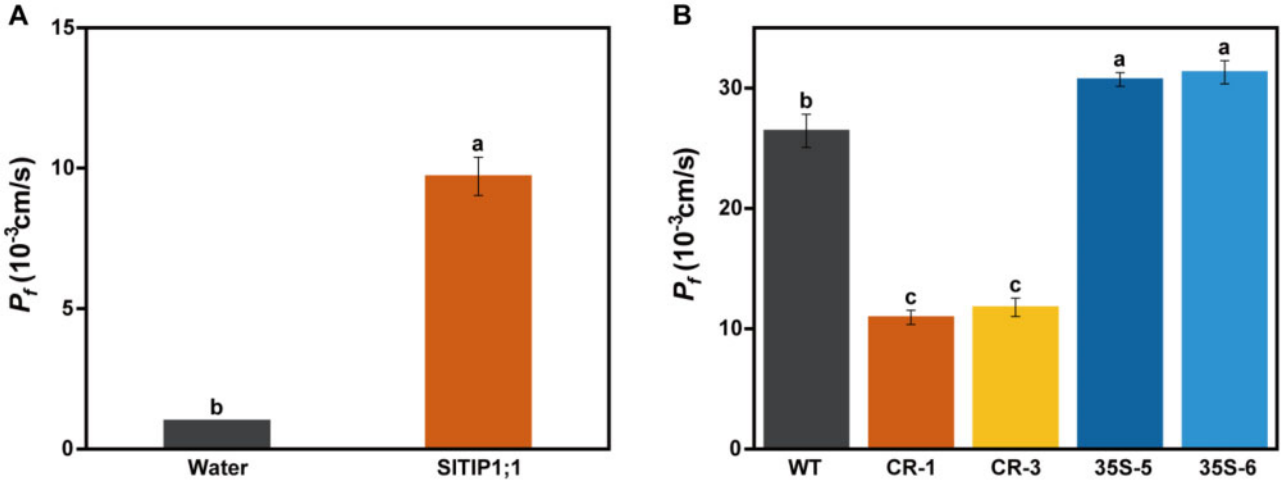

Figure 12 *SlTIP1;1* mediates water transport in *X. laevis* oocytes and the AZ. A, Osmotic water permeability coefficient (P_f) of oocytes injected with water (control) and *SlTIP1;1* cRNA. The amount of cRNA (ng) used is shown to the left. Values (P_f) are expressed as means of measurements from three independent experiments ± SD, with two to four samples per replicate. B, The P_f of the WT, *35S:SlTIP1;1* (35S-5, 35S-6), and *CRsltip1;1*(CR-1, CR-3) AZs. Different lowercase letters indicate significant differences in means (Student's *t* test, $P < 0.05$).

The role of *SlTIP1;1* in modifying the AZ auxin and ETH signal during pedicel abscission

Manipulation of auxin concentrations in the AZ cells of Arabidopsis flowers revealed that the loss of auxin in the AZ is a requirement for triggering abscission (Basu et al., 2013). During flower removal-induced abscission, a rapid downregulation in the expression of the auxin response genes *IAA*1, *IAA*3, and *IAA*4, and a slow downregulation of *IAA*8 and *IAA*9, in parallel with an increase in the AZ ROS levels, have been observed (Meir et al., 2010; Bar-Dror et al., 2011), occurring with the initiation of pedicel abscission, but before the development of increased ETH sensitivity in AZ cells. Moreover, chilling or high light after chilling has also been reported to induce leaf abscission via IAA peroxidation (Michaeli et al., 2001). During ETH-induced abscission in flower pedicels of *Nicotiana tabacum*, a significant increase in Prx activity was observed in the first 4 h, in contrast to non-ETH-treated tissues (Henry and Jensen, 1973). Strong H_2O_2 signals have been reported in the cytoplasm during abscission, and Prxs have been observed in the cell wall, ER, vacuoles, and the plasma membrane during different types of abscission (Henry and Jensen, 1973; Meir et al., 2006; Cai and Lashbrook, 2008). In this study, blocking the entry of H_2O_2 into the cytoplasm led to stronger auxin responses, as suggested by the DR5::VENUS in the *CRsltip1;1* line (Figure 9, A and B). The *CRsltip1;1* line showed a lower abscission rate under auxin treatment, whereas *35S:SlTIP1;1* showed a higher abscission rate compared to the wild-type (Figure 9C). We propose that elevated cytoplasmic H_2O_2 in the early abscission stage (4 h) induces Prxs, which interfere with the AZ intracellular auxin homeostasis by degrading free auxin. Hence, H_2O_2 transport into the cytoplasm mediated by *SlTIP1;1* in the early stage is important for initial abscission.

H_2O_2 is an effective inducer of ETH production (Ke and Sun, 2004; Qin et al., 2008). Interestingly, pepper (*Capsicum annuum*) flowers with osmotic stress were reported to have elevated ETH production and accelerated abscission, while the addition of ROS scavengers significantly depressed ETH production and delayed abscission (Jaafar et al., 1998). We observed that the KO lines produced less ETH, and the overexpression lines had higher ETH production, compared to the wild type (Figure 10). DPI significantly reduced ETH production in the wild-type and the *35S:SlTIP1;1* line. Under the H_2O_2 treatment, *35S:SlTIP1;1* had higher and *CR-sltip1;1* had lower ETH production in comparison to the wild-type. The above results verify the role of *SlTIP1;1* in gating cytoplasmic H_2O_2 and enhancing ETH production during abscission.

Some key ETH elements, such as *SlETR1*, *SlCTR14*, *SlETR3* (*NR*), and *SlERF52*, have been identified in ETH-dependent abscission (Leclercq et al., 2002; Whitelaw et al., 2002; Nakano et al., 2014; Wang et al., 2018). The in vivo and in vitro assays in our study which indicated that SlERF52 directly regulated *SlTIP1;1* expression and the *SlTIP1;1* KO line, insensitive to ETH-induced abscission, suggested an important biological role of ETH: ETH is involved in the employment of SlERF52 to fine-tune *SlTIP1;1* expression so as to accelerate tomato pedicel abscission (Figure 11). Because of the high accumulation of SlTIP*1;1*, a positive feedback in the ETH signal, via a H_2O_2-dependent pathway, is then created.

SlTIP1;1-dependent water influx is required for pedicel abscission

Water transport to the AZ for cell expansion and the possible importance of AQPs has been discussed in detail in recent literature. An *ida* mutant, showing a defect in flower organ abscission, might be a result of IDA signals affecting water relations of the AZ cells via AQPs (Meir et al., 2019). Limited cell expansion and cell wall disruption leads to a delay in abscission, and downregulation of the cell wall expansin gene, *AtEXP10*, inhibits Arabidopsis flower organ

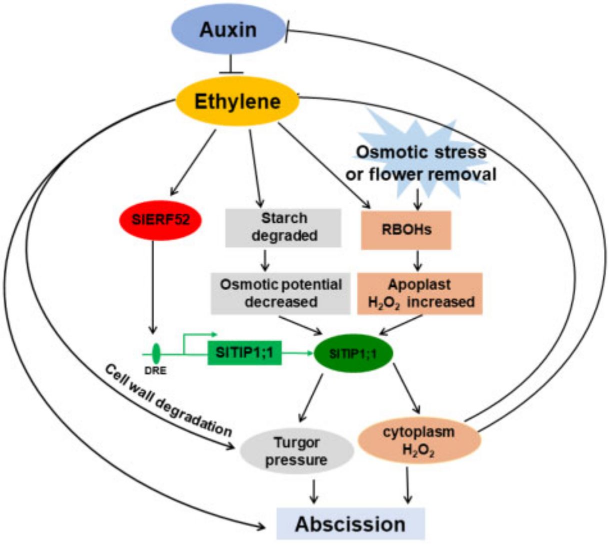

Figure 13 Model showing SlERF52-*SlTIP1;1* regulatory module that functions as an accelerator of pedicel abscission by increasing cytoplasmic H_2O_2 and osmotic water permeability.

abscission (Hyung-Taeg and Cosgrove, 2000). Antisense downregulation of *TAPG4* endo1,4-β-glucanase in tomato is also known to inhibit flower pedicel abscission (Cai-Zhong et al., 2008). However, in the *nev* mutant, in which floral abscission is blocked, there is a higher expansion rate in the AZ cells, indicating that cell expansion alone is not sufficient to trigger abscission (Liu et al., 2013). We found that, as compared to the wild-type, the *CRtip1;1* line had lower AZ cell P_f, while the *35S:SlTIP1;1* line had higher AZ cell P_f (Figure 12). Using the ROS scavenger DPI to eliminate the difference in ROS levels in wild-type, *35S:SlTIP1;1*, and *CRtip1;1* led to *35S:SlTIP1;1* showing significantly accelerated abscission, in contrast to *CRtip1;1* explants, after 32 h but not before 24 h. The results indicate that *SlTIP1;1*, dependent on the rate of water transport, is required for the final stage of abscission.

In summary, our results suggest a model in which osmotic stress or flower removal enhances the level of apoplastic H_2O_2 in the pedicel AZ, which is then transported into the cytoplasm via *SlTIP1;1*. The elevated cytoplasmic H_2O_2 concentration in turn suppresses auxin signals in the early stage of abscission and then enhances ETH production. ETH activates SlERF52-induced *SlTIP1;1* expression, thus leading to elevated levels of cytoplasmic H_2O_2 and water influx, accelerating abscission (Figure 13).

Materials and methods

Plant materials and growth conditions

Wild type tomato (*S. lycopersicum* L. cv Zhongshu 6) and transgenic lines, grown as previously described (Wang et al., 2018), were used for the study.

Abscission assay

Pedicel explants were obtained from newly opened tomato flowers and incubated in double distilled water (control) or AXS (1 mM KH_2PO_4, 1 mM K_2HPO_4, 1 mM $CaCl_2$, 0.1 mM $MgSO_4$, 3 mM KNO_3, and 0.1 mM $MnSO_4$ buffered to pH 5.8 with 1 M HCl or KOH), or 0.02 and 0.03 μM $HgCl_2$, or 5 and 10 mM phloretin. For 1-MCP treatment, the plants were exposed to 1-MCP (0.5 $\mu L\ L^{-1}$) in a sealed 100 L chamber at 25°C for 10 h before flower removal. Abscission assays were performed as previously described (Wang et al., 2005).

Liquid chromatography–tandem mass spectrometry and data analysis

Liquid chromatography–tandem mass spectrometry analysis was performed using a Q Exactive Mass Spectrometer (Thermo Scientific) coupled to an Easy nLC (Proxeon Biosystems, now Thermo Fisher Scientific) for 60 min by the Applied Protein Technology company (Shanghai, China). MS data were acquired using a data-dependent top10 method, dynamically choosing the most abundant precursor ions from the survey scan (300–1,800 m/z) for higher energy collisional dissociation (HCD) fragmentation. Survey scans were acquired at a resolution of 70,000 at m/z 200, and resolution for HCD spectra was set to 17,500 at m/z 200, with an isolation width of 2 m/z. The MS data were analyzed using MaxQuant software version 1.5.3.17 (Max Planck Institute of Biochemistry in Martinsried, Germany). MS data were searched against the UniProtKB plant database (2,585,998 total entries, downloaded July 6, 2012). The cutoff of the global false discovery rate for peptide and protein identification was set to 0.01. The matching sequence of tomato AQP homologs are listed in Supplemental Table S1.

In situ hybridizations

In situ hybridization analysis of *SlTIP1;1* was performed as previously described (Wang et al., 2018). Antisense and sense RNA probes were labeled using a DIG RNA-labeling kit (Roche). Probes for *SlTIP1;1* ranged from 268 to 572 bp, including the unique region. Samples were collected from different abscission stages of the AZs, and hybridization with DIG-labeled probes was performed as previously described (Guerin et al., 2000).

Reverse transcription quantitative PCR (qPCR)

RNA extraction was performed from the AZ and the NAZ of the wild-type and the *CRsltip1;1* transgenic tomato line at different time points (0, 4, 8, 16, 20, 24, and 32 h). The AZ and NAZ tissues were sampled as previously described (Meir et al., 2010). First-strand cDNA was synthesized using M-MLV reverse transcriptase according to the manufacturer's instructions, using oligo (dT) primers (Takara). RT-qPCR was performed with a SYBR Green PCR Master Mix kit (Takara) using an ABi7500 instrument (Applied Biosystems). Actin gene was used as an internal control and total RNA was extracted from three groups of AZ and NAZ, as mentioned above, as three biological replicates. Relative quantification of the expression of each gene was performed using the $2^{-\Delta\Delta CT}$ method. The primers are listed in Supplemental Table S2.

Localization of *SlTIP1;1*

Arabidopsis (*Arabidopsis thaliana*; ecotype Columbia) mesophyll protoplasts were generated from rosette leaves of 4 weeks old plants and transiently transformed as described in Yoo et al. (2007). The transformed protoplasts were incubated in the dark for 16 h at 20°C. The subcellular distribution of *SlTIP1;1*, tagged with GFP and expressed in Arabidopsis mesophyll protoplasts, was visualized by confocal microscopy (Leica SP8, Leica Microsystems, Germany). For immunogold staining, the AZ samples were fixed using O_5O_4 and embedded in LR white. After embedding in gelatin capsules, polymerization was performed at 60°C for 2 d. Samples were cut into ultrathin sections (50 nm), and blocked in 2% (w/v) bovine serum albumin, before a 1:100 primary antibody of *SlTIP1;1* diluted in phosphate-buffered saline (PBS) was added at 4°C to cover the sections overnight. The sections were then washed three times in a PBS-Tween-20 solution and incubated with immunogold reagent (15 nm gold, Bio-Rad, USA) at 37°C for 1 h. The labeled samples were then imaged by using a HT 7700 transmission electron microscope at an accelerating voltage of 75 kV (Hitachi, Tokyo, Japan).

Western blot

The primary antibody targeting *SlTIP1;1* was generated by the Abmart Company (China) by injecting synthetic *SlTIP1;1* peptides separately (Supplemental Table S2). Anti-40 S and secondary antibodies were obtained from the Kangwei Company (China). For the western blot analysis, proteins were extracted from the AZ and visualized as described previously (Tao et al., 2015). The electrophoretically separated proteins were transferred to Polyvinylidene fluoride (PVDF) membranes using the Trans-BlotTurbo^{TM} transfer system (Bio-Rad, USA) according to the manufacturer's instructions. The PVDF membranes were incubated for 8 h or overnight at 4°C with diluted (1:1,000) primary antibody of *SlTIP1;1*. After three washes, the membranes were incubated with the secondary antibody at room temperature for 1 h. The signal was observed and imaged on the Azure c600 western blot imaging system (Azure, USA).

35S:SlTIP1;1 plasmid construction

The full-length *SlTIP1;1* sequence cDNA was first amplified using gene-specific primers. Full-length *SlTIP1;1* was cloned into the pENTR/D-TOPO vector (Invitrogen) using BP clonase (Invitrogen) and then into the binary vector pB7YWG2 using LR clonase (Invitrogen).

Generation and genotyping of CRISPR plants

Two 19-bp fragments from the *SlTIP1;1* CDS (153–171 and 374–392 bp) were chosen as target sequences for genome editing of *SlTIP1;1*. The target guide RNA (gRNA) sequences were obtained by PCR using the pHSE401 vector as a template combined with forward and reverse primers containing the gRNAs. The U6-26-*SlTIP1;1*-gRNA cassettes were cloned into the CRISPR/Cas9 binary vector, pCBC-DT1T2_tomatoU6, to generate pCBC-DT1T2_tomatoU6-*SlTIP1;1*. The plasmids were introduced into *Agrobacterium tumefaciens* strain LB4404, and transformation of tomato (*S. lycopersicum*) Ailsa Craig (AC) was performed according to the methodology of Wang et al. (2018). Overexpression and mutations were identified by PCR analysis and DNA sequencing. Cas9-free T2 plants carrying mutations were screened and identified.

Protoplast isolation

The manual longitudinal sections (about 50-µm thickness) of the wild-type and transgenic pedicel AZs were placed onto polyethylene naphthalate membrane-coated slides (Zeiss Micro-imaging). The AZ samples were obtained using a PALM MicroBeam system (Carl Zeiss, Germany; Supplemental Figure S1). The laser energy was set to 78 (scale from 0 to 100) and the laser focus was set to 70 (scale from 0 to 100). The excised AZ cells were catapulted and collected into the caps of 0.5-mL Eppendorf vials containing an enzyme solution (1.2% (w/v) cellulase R-10 (Yakult, Japan), 0.6% (w/v) macerozyme R-10 (Yakult, Japan), 530 mM mannitol, 8 mM MES, pH 5.8). The samples were incubated for 30 min at 28°C. Then, they were transferred to a similar solution but without enzymes, and centrifuged at 200 *g* for 5 min. Protoplasts were removed, diluted with 10 mL of the mannitol solution, and pelleted by centrifugation at 300*g* for 2 min.

Functional analysis of *SlTIP1;1* in yeast

For the H_2O_2 growth assay, *Saccharomyces cerevisiae* BY4741 and the H_2O_2 tolerant mutant strain *yca1* were obtained from Euroscarf (Frankfurt, Germany). The full-length *SlTIP1;1* sequence was cloned into the *pYES2.0* vectors. The full-length *AtPIP2;4* cDNA from Arabidopsis was used to identify the H_2O_2 transport capacity of AQPs, which were cloned into *pYES2.0* as a positive control. Yeast viability assays under H_2O_2 treatment were performed as described by Sadhukhan et al. (2017). The yeast strain transformed with empty vectors or vectors containing the different AQP genes were inoculated in liquid yeast nitrogen base with 2% (w/v) glucose, 30 mg L^{-1} histidine and methionine, and 90 mg L^{-1} leucine (excluding uracil), with a pH of 5.7. Yeast cells were collected at an optical density of OD_{600} of 1.0. Cultures were diluted in five-fold serial dilutions and spotted on selection media containing 0, 1.5, or 2 mM H_2O_2. The colonies were counted after 120-h incubation at 30°C.

H_2O_2 measurement

For AZ H_2O_2 detection, different AZs at different stages were excised and immediately incubated in 50 mM pH 7.4 phosphate buffer for 10 min to remove wounding-induced ROS. The samples were then incubated in AR or AUR solution for 0.5 h. The AR and AUR positive signals were then measured at 585–610 nm using 525 nm excitation with a Leica SP8 confocal microscope. Apoplastic and cytoplasmic signals were quantified using ImageJ software.

AZ protoplast ROS signals were investigated following previously reported protocols (Wang et al., 2009). AZ protoplasts were first incubated in a H_2DCFDA solution for 30 min and then treated with H_2O_2 before the signal was recorded using a Leica SP8 laser scanning confocal microscope. The H_2DCFDA fluorescence intensities in AZ protoplasts were quantified using Image J. At least 200 AZ protoplasts were analyzed.

Microscope observation

Using a Leica SP8 confocal microscope, Z-stacks were scanned every 1.5 μm in thickness and maximum projections were generated. Imaging of VENUS was done at 510–550 nm and bright field was regarded as a control.

Measurement of ETH production

ETH production was carried out in three biological replicates as previously described (Roberts et al., 1984). Approximately, 12 pedicel AZ samples were assessed for each biological replicate; they were placed in a sealed 50 mL glass jar, and after 1 h, 1 mL of gas was removed from the headspace with a syringe. The gas was analyzed by gas chromatography using a Varian GC-3800 equipped with a GDX-102 column (Dalian Institute of Chemical Physics, China), with nitrogen (20 mL min^{-1}) as the carrier gas.

Electrophoretic mobility shift assays

The full-length *SlERF52* sequence was cloned into the pET30 vector and expressed in Rosetta *Escherichia coli* cells. After induction with 1 mM IPTG for 6 h, SlERF52 was purified using Ni-NTP Spin Columns (Qiagen, Germany). The double-stranded DNA probe was prepared by annealing complementary oligonucleotides, and the biotin-labeled *SlTIP1;1* promoter was shown in Figure 11. The different AQP DNA fragments were labeled at their respective 5′-ends with biotin by the Life Company (Shanghai, China). DNA binding assays were performed as previously described (Li et al., 2016).

β-glucuronidase (GUS) analysis

The promoter sequences of *SlTIP1;1* (404-bp upstream of the start ATG) were cloned into the *Sac*I and *Sma*I sites upstream of the GUS reporter gene in the pBI101 vector to generate a reporter construct. Mutations were introduced into the drought-responsive element of the *SlTIP1;1* promoter employing a Fast Mutagenesis System kit (Transgen Biotech, China). For the effector construct, the full-length *SlERF52* sequence was introduced into the pRI101 vector using restriction enzymes *Nco*I and *Bam*HI. The infiltration of reporter and effector constructs into tobacco leaves and GUS labeling were performed according to Li et al. (2016).

Y1H assays

The full-length *SlERF52* sequence was ligated into the *pGADT7* vector to generate the *AD-SlERF52* construct, and the AQP promoter fragments were ligated into the *pAbAi* vector. Y1H assays were conducted using a Gold Yeast One-Hybrid Library Screening System kit (Clontech, USA) according to the manufacturer's protocols. The yeast growth assays were performed at least three independent times, with consistent results.

Expression in *X. laevis* oocytes and water permeability assay

The coding region of *SlTIP1;1* was cloned into the *pGEMHE* vector. Complementary RNAs (cRNAs) were synthesized using the T7 RiboMAX Large Scale RNA Production System (Promega, Madison, USA). *Xenopus laevis* oocytes were isolated and injected with 50-nL distilled water (control) or *SlTIP1;1* cRNA (12 ng in 50 nL). The oocytes were then cultivated at 17°C for 3 d in Barth's solution supplemented with 100 μg mL^{-1} streptomycin and 50 μg mL^{-1} gentamycin sulfate. The osmotic water permeability (P_f) was determined according to the rate of increase in the volume of oocytes after transfer to 1/5 diluted Barth's solution and recording using video microscopy (Zeiss Observer. A1). P_f was calculated according to the following equation:

$$P_f = V_0[d(V/V_0)/dt]/[S \times V_w(Osm_{in} - Osm_{out})],$$

where V_0 represents the initial oocyte volume and S represents the initial oocyte surface. The molar volume of water (V_w) is 18 cm^3 mol^{-1} (Zhang and Verkman, 1991).

AZ protoplast P_f assay

P_f was determined based on the rate of volume increase in protoplasts when they were transferred from a 600 mOsmol isotonic solution to a 500 mOsmol hypotonic solution. P_f was determined using the Matlab fitting program P_f FIT, as described in Shatil-Cohen et al. (2014).

Accession numbers

Sequence data from this article can be found in the Genome Database for Tomato (https://www.solgenomics.net/) or GenBank/EMBL libraries under accession numbers SlPIP1;3 (AB845606), SlPIP1;5 (AB845607), SlPIP1;7 (AB845608), SlPIP2;4 (AB845610), SlPIP2;5 (AB845611), SlTIP1;1 (AB845616), SlTIP4;1 (AB845624), SlNIP5;1 (AB845630), SlERF52 (101266617), and Actin (X55749).

Supplemental data

Supplemental Figure S1. An abscission zone (AZ) sample, obtained using the PALM MicroBeam system.

Supplemental Figure S2. Quantification of *SlTIP1;1* in 35S: *SlTIP1;1* and wild-type (WT) pedicel abscission zones (AZs).

Supplemental Figure S3. DNA sequences of CRISPR/Cas9 target sites in the stable knockout *SlTIP1;1* tomato line.

Supplemental Table S1. Mass spectrometry analysis of peptides isolated from a fraction containing proteins in the size range of 25 to 32 kDa and matching the sequence of tomato aquaporin homologs.

Supplemental Table S2. The primers used in this study.

Acknowledgments

We thank the experimental conditions provided by the laboratory of Academician Weihua Wu (State Key Laboratory of Plant Physiology and Biochemistry, College of Biological Sciences, China Agricultural University, China) for completing the *X. laevis* oocytes experiment, and thank PlantScribe (www.plantscribe.cm) for editing this manuscript.

Funding

This work was supported by the National Key Research and Development Program of China (grant number 2018YFD1000800), the National Natural Science Foundation of China (grant numbers 31572167, 31672197, U1708232, 31861143045), the Liaoning Revitalization talent program (2018050), and China Scholarship Council.

Conflicts of interest statement. The authors declare no conflicts of interest.

References

Addicott FT (1982) Abscission. University of California Press, Berkeley, CA.

Agati G, Azzarello E, Pollastri S, Tattini M (2012) Flavonoids as antioxidants in plants: location and functional significance. Plant Sci **196**: 67–76

Bar-Dror T, Dermastia M, Kladnik A, Žnidarič MT, Novak MP, Meir S, Burd S, Philosoph-Hadas S, Ori N, Sonego L (2011) Programmed cell death occurs asymmetrically during abscission in tomato. Plant Cell **23**: 4146–4163

Bashandy T, Guilleminot J, Vernoux T, Caparros-Ruiz D, Ljung K, Meyer Y, Reichheld JP (2010) Interplay between the NADP-linked thioredoxin and glutathione systems in Arabidopsis auxin signaling. Plant Cell **22**: 376–391

Basu MM, Gonzalez-Carranza ZH, Azam-Ali S, Tang S, Shahid AA, Roberts JA (2013) The manipulation of auxin in the abscission zone cells of Arabidopsis flowers reveals that indoleacetic acid signaling is a prerequisite for organ shedding. Plant Physiol **162**: 96–106

Beebo A, Thomas D, Der C, Sanchez L, Leborgne-Castel N, Marty F, Schoefs BT, Bouhidel K (2009) Life with and without AtTIP1;1, an Arabidopsis aquaporin preferentially localized in the apposing tonoplasts of adjacent vacuoles. Plant Mol Biol **70**: 193–209

Bellati J, Alleva K, Soto G, Vitali V, Jozefkowicz C, Amodeo G (2010) Intracellular pH sensing is altered by plasma membrane PIP aquaporin co-expression. Plant Mol Biol **74**: 105–118

Bienert GP, Bienert MD, Jahn TP, Boutry M, Chaumont F (2011) Solanaceae XIPs are plasma membrane aquaporins that facilitate the transport of many uncharged substrates. Plant J **66**: 306–317

Bienert GP, Chaumont F (2014) Aquaporin-facilitated transmembrane diffusion of hydrogen peroxide. Biochim Biophys Acta **1840**: 1596–1604

Blomster T, Salojarvi J, Sipari N, Brosche M, Ahlfors R, Keinanen M, Overmyer K, Kangasjarvi J (2011) Apoplastic reactive oxygen species transiently decrease auxin signaling and cause stress-induced morphogenic response in Arabidopsis. Plant Physiol **157**: 1866–1883

Braidwood L, Breuer C, Sugimoto K (2013) My body is a cage: mechanisms and modulation of plant cell growth. New Phytol **201**: 388–402

Butenko MA, Patterson SE, Grini PE, Stenvik G-E, Amundsen SS, Mandal A, Aalen RB (2003) Inflorescence deficient in abscission controls floral organ abscission in Arabidopsis and identifies a novel family of putative ligands in plants. Plant Cell **15**: 2296–2307

Cai S, Lashbrook CC (2008) Stamen abscission zone transcriptome profiling reveals new candidates for abscission control: enhanced retention of floral organs in transgenic plants overexpressing Arabidopsis ZINC FINGER PROTEIN2. Plant Physiol **146**: 1305–1321

Cai-Zhong J, Feng L, Wachiraya I, Shimon M, Michael SR (2008) Silencing polygalacturonase expression inhibits tomato petiole abscission. J Exp Bot **59**: 973–979

Caiqin L, Yan W, Xuming H, Jiang L, Huicong W, Jianguo L (2015) An improved fruit transcriptome and the identification of the candidate genes involved in fruit abscission induced by carbohydrate stress in litchi. Front Plant Sci **6**: 439

Chaoui A, Ferjani EE (2005) Effects of cadmium and copper on antioxidant capacities, lignification and auxin degradation in leaves of pea (Pisum sativum L.) seedlings. C R Biol **328**: 23–31

Chaumont FO, Barrieu FO, Chrispeels HM (1998) Characterization of a maize tonoplast aquaporin expressed in zones of cell division and elongation. Plant Physiol **117**: 1143–1152

Corbacho J, Romojaro F, Pech J-C, Latché A, Gomez-Jimenez MC (2013) Transcriptomic events involved in melon mature-fruit abscission comprise the sequential induction of cell-wall degrading genes coupled to a stimulation of endo and exocytosis. PLoS One **8**: e58363.

Damodharan S, Zhao D, Arazi T (2016) A common miRNA160-based mechanism regulates ovary patterning, floral organ abscission and lamina outgrowth in tomato. Plant J **86**: 458–471

Day A, Veal E (2011) Hydrogen peroxide as a signaling molecule. Antioxid Redox Signal **15**: 147–151

Dimitrov PV, Frank VB (2012) Hydrogen peroxide—a central hub for information flow in plant cells. AoB Plants **2012**: pls014

Djanaguiraman M, Durga Devi D, Sheeba JA, Bangarusamy U, Babu RC (2004) Effect of oxidative stress on abcission of tomato fruits and its regulation by Nitrophenols. Ann Clin Lab Sci **1**: 134–138

Elobeid M, Polle A (2012) Metal Toxicity in Plants: Perception, Signaling and Remediation. Springer, Berlin/Heidelberg, Germany, pp 249–259

Guerin J, Rossel JB, Robert S, Tsuchiya T, Koltunow A (2000) A DEFICIENS homologue is down-regulated during apomictic initiation in ovules of Hieracium. Planta **210**: 914–920

Hacke UG, Jacobsen AL, Pratt RB, Maurel C, Lachenbruch B, Zwiazek J (2012) New research on plant-water relations examines the molecular, structural, and physiological mechanisms of plant responses to their environment. New Phytol **196**: 345–348

Henry EW, Jensen TE (1973) Peroxidases in tobacco abscission zone tissue. J Cell Sci **13**: 591–601

Hooijmaijers C, Rhee JY, Kwak KJ, Chung GC, Horie T, Katsuhara M, Kang H (2012) Hydrogen peroxide permeability of plasma membrane aquaporins of Arabidopsis thaliana. J Plant Res **125**: 147–153

Hyung-Taeg C, Cosgrove DJ (2000) Altered expression of expansin modulates leaf growth and pedicel abscission in Arabidopsis thaliana. Proc Natl Acad Sci U S A **97**: 9783–9788

Jaafar H, Atherton J, Black C, Roberts J (1998) Impact of water stress on reproductive development of sweet peppers (Capsicum annuum L.). I. Role of ethylene in water deficit-induced flower abscission. J Trop Agric Food Sci **26**: 165–174

Jang JY, Rhee JY, Chung GC, Kang H (2011) Aquaporin as a membrane transporter of hydrogen peroxide in plant response to stresses. Plant Signal Behav **7**: 1180–1181

Johansson I, Karlsson M, Johanson U, Larsson C, Kjellbom P (2000) The role of aquaporins in cellular and whole plant water balance. Biochim Biophys Acta **1465**: 324–342

Ke D, Sun G (2004) The effect of reactive oxygen species on ethylene production induced by osmotic stress in etiolated mungbean seedling. Plant Growth Regul **3**: 199–206

Kovtun YI, Chiu WL, Tena G (2000) Functional analysis of oxidative stress-activated mitogen-activated protein kinase cascade in plants. Proc Natl Acad Sci U S A **97**: 2940–2945

Kumpf RP, Shi CL, Larrieu A, Stø IM, Aalen RB (2013) Floral organ abscission peptide IDA and its HAE/HSL2 receptors control cell separation during lateral root emergence. Proc Natl Acad Sci U S A **110**: 5235–5240

Leclercq J, Adams-Phillips LC, Zegzouti H, Jones B, Latché A, Giovannoni JJ, Pech J-C, Bouzayen M (2002) LeCTR1, a tomato CTR1-like gene, demonstrates ethylene signaling ability in Arabidopsis and novel expression patterns in tomato. Plant Physiol **130**: 1132–1142

Lers A, Sonego L, Green PJ, Burd S (2006) Suppression of LX ribonuclease in tomato results in a delay of leaf senescence and abscission. Plant Physiol **142**: 710–721

Li T, Jiang Z, Zhang L, Tan D, Wang A (2016) Apple (Malus domestica) MdERF2 negatively affects ethylene biosynthesis during fruit ripening by suppressing MdACS1 transcription. Plant J **88**: 735–748

Liang Q, Li W, Zhou B (2008) Caspase-independent apoptosis in yeast. Biochim Biophys Acta **1783**: 1311–1319

Liao W, Wang G, Li Y, Wang B, Zhang P, Peng M (2016) Reactive oxygen species regulate leaf pulvinus abscission zone cell separation in response to water-deficit stress in cassava. Sci Rep **6**: 21542

Liu B, Butenko MA, Shi C-L, Bolivar JL, Winge P, Stenvik G-E, Vie AK, Leslie ME, Brembu T, Kristiansen W (2013) NEVERSHED and INFLORESCENCE DEFICIENT IN ABSCISSION are differentially required for cell expansion and cell separation during floral organ abscission in Arabidopsis thaliana. J Exp Bot **64**: 5345–5357

Lloyd J, Howie H, Lloyd J, Howie H (1989) Response of orchard 'Washington Navel' orange, Citrus sinensis (L.) Osbeck, to saline irrigation water. I. Canopy characteristics and seasonal patterns in leaf osmotic potential, carbohydrates and ion concentrations. Aust J Agric Res **40**: 359–369

Luu DT, Maurel C (2013) Aquaporin trafficking in plant cells: an emerging membrane-protein model. Traffic **14**: 629–635

Ma C, Meir S, Xiao L, Tong J, Liu Q, Reid MS, Jiang C-Z (2015) A KNOTTED1-LIKE HOMEOBOX protein regulates abscission in tomato by modulating the auxin pathway. Plant Physiol **167**: 844–853

Meir S, Hunter DA, Chen J-C, Halaly V, Reid MS (2006) Molecular changes occurring during acquisition of abscission competence following auxin depletion in Mirabilis jalapa. Plant Physiol **141**: 1604–1616

Meir S, Philosoph-Hadas S, Sundaresan S, Selvaraj KV, Burd S, Ophir R, Kochanek B, Reid MS, Jiang C-Z, Lers A (2010) Microarray analysis of the abscission-related transcriptome in the tomato flower abscission zone in response to auxin depletion. Plant Physiol **154**: 1929–1956

Meir S, Philosoph-Hadas S, Riov J, Tucker ML, Patterson SE, Roberts JA (2019) Re-evaluation of the ethylene-dependent and-independent pathways in the regulation of floral and organ abscission. J Exp Bot **70**: 1461–1467

Menghan S, Anh TP, Marta SI, Belay TA (2018) Ethylene regulates post-germination seedling growth in wheat through spatial and temporal modulation of ABA/GA balance. J Exp Bot **71**: 1985–2004

Merelo P, Agustí J, Arbona V, Costa ML, Estornell LH, Gómez-Cadenas A, Coimbra S, Gómez MD, Pérez-Amador MA, Domingo C, et al. (2017) Cell wall remodeling in abscission zone cells during ethylene-promoted fruit abscission in citrus. Front Plant Sci **8**: 126

Michaeli R, Philosophhadas S, Riov J, Shahak Y, Ratner K, Meir S (2001) Chilling-induced leaf abscission of Ixora coccinea plants. III. Enhancement by high light via increased oxidative processes. Physiol Plant **113**: 338–345

Miller G, Suzuki N, Ciftci-Yilmaz S, Mittler R (2010) Reactive oxygen species homeostasis and signalling during drought and salinity stresses. Plant Cell Environ **33**: 453–467

Najeeb U, Tan DKY, Bange MP (2015) Inducing waterlogging tolerance in cotton via an anti-ethylene agent aminoethoxyvinylglycine application. Arch Agron Soil Sci **62**: 1136–1146

Nakano T, Fujisawa M, Shima Y, Ito Y (2014) The AP2/ERF transcription factor SlERF52 functions in flower pedicel abscission in tomato. J Exp Bot **65**: 3111–3119

Niederhuth CE, Patharkar OR, Walker JC (2013) Transcriptional profiling of the Arabidopsis abscission mutant hae hsl2 by RNA-Seq. BMC Genomics **14**: 37–37

Park SY, Park JC, Kim MS, Lee SE, Kim KJ, Jung BJ, Park W, Jeon DW, Cho KS, Kim CS (2015) Differential effect of water-soluble chitin on collagen synthesis of human bone marrow stem cells and human periodontal ligament stem cells. Tissue Eng Part A **21**: 451

Patharkar OR, Walker JC (2015) Floral organ abscission is regulated by a positive feedback loop. Proc Natl Acad Sci U S A **112**: 2906–2911

Paz M, Javier A, Vicent A, Costa ML, Estornell LH, Aurelio G-C, Silvia C, Gómez MD, Pérez-Amador MA, Concha D, et al. (2017) Cell wall remodeling in abscission zone cells during ethylene-promoted fruit abscission in citrus. Front Plant Sci https://doi.org/10.3389/fpls.2017.00126

Qin Y-M, Hu C-Y, Zhu Y-X (2008) The ascorbate peroxidase regulated by H2O2 and ethylene is involved in cotton fiber cell elongation by modulating ROS homeostasis. Plant Signal Behav **3**: 194–196

Reisen D, Leborgne-Castel N, Zalp C, Chaumont F, Marty F (2003) Expression of a cauliflower tonoplast aquaporin tagged with GFP in tobacco suspension cells correlates with an increase in cell size. Plant Mol Biol **52**: 387–400

Rigal A, Doyle SM, Robert S (2015) Live cell imaging of FM4-64, a tool for tracing the endocytic pathways in Arabidopsis root cells. Methods Mol Biol **1242**: 93–103

Roberts JA, Schindler CB, Tucker GA (1984) Ethylene-promoted tomato flower abscission and the possible involvement of an inhibitor. Planta **160**: 159–163

Sadhukhan A, Kobayashi Y, Nakano Y, Iuchi S, Kobayashi M, Sahoo L, Koyama H (2017) Genome-wide association study reveals that the aquaporin NIP1;1 contributes to variation in hydrogen peroxide sensitivity in Arabidopsis thaliana. Mol Plant **10**: 1082–1094

Sakamoto M, Munemura I, Tomita R, Kobayashi K (2008) Involvement of hydrogen peroxide in leaf abscission signaling, revealed by analysis with an in vitro abscission system in Capsicum plants. Plant J **56**: 13–27

Schüssler MD, Alexandersson E, Bienert GP, Kichey T, Jahn TP (2010) The effects of the loss of TIP1;1 and TIP1;2 aquaporins in Arabidopsis thaliana. Plant J **56**: 756–767

Shatil-Cohen A, Sibony H, Draye X, Chaumont F, Moran N, Moshelion M (2014) Measuring the osmotic water permeability coefficient (Pf) of spherical cells: isolated plant protoplasts as an example. J Vis Exp **92**: 1–13

Srivignesh S, Sonia P-H, Joseph R, Eduard B, Betina K, Mark LT, Shimon M (2015) Abscission of flowers and floral organs is closely associated with alkalization of the cytosol in abscission zone cells. J Exp Bot **66**: 1355–1368

Steffens B, Sauter M (2009) Epidermal cell death in rice ss confined to cells with a distinct molecular identity and is mediated by ethylene and H_2O_2 through an autoamplified signal pathway. Plant Cell **1**: 184–196

Swaef TD, Steppe K (2010) Linking stem diameter variations to sap flow, turgor and water potential in tomato. Function Plant Biol **37**: 429–438

Tabuchi T, Ito S, Arai N (2001) Anatomical studies of the abscission process in the tomato pedicels at flowering stage. J Jpn Soc Hortic Sci **70**: 63–65

Tao X, Yanling W, Xin L, Song G, Mingfang Q, Tianlai L (2015) Solanum lycopersicum IAA15 functions in the

2,4-dichlorophenoxyacetic acid herbicide mechanism of action by mediating abscisic acid signalling. J Exp Bot **66**: 3977–3990

Taras P, Geert P, Roland C, Jansen MAK (2005) Complementary interactions between oxidative stress and auxins control plant growth responses at plant, organ, and cellular level. J Exp Bot **56**: 1991–2001

Tian S, Wang X, Li P, Wang H, Ji H, Xie J, Qiu Q, Shen D, Dong H (2016) Plant aquaporin AtPIP1;4 links apoplastic H2O2 induction to disease immunity pathways. Plant Physiol **171**: 1635–1650

Tranbarger TJ, Tucker ML, Roberts JA, Shimon M (2017) Editorial: plant organ abscission: from models to crops. Front Plant Sci **8**: 196

Tucker ML, Sexton R, DelCampillo E, Lewis LN (1988) Bean abscission cellulase: characterization of a cDNA clone and regulation of gene expression by ethylene and auxin. Plant Physiol **88**:1257–1262

Wang LL, Chen AP, Zhong NQ, Liu N, Wu XM, Wang F, Yang CL, Romero MF, Xia GX (2014) The thellungiella salsuginea tonoplast aquaporin TsTIP1;2 functions in protection against multiple abiotic stresses. Plant Cell Physiol **55**: 148–161

Wang LL, Zheng SS, Tong PP, Chen Y, Liu WZ (2016) Cytochemical localization of H_2O_2 in pigment glands of cotton(Gossypium hirsutum L.). J Integr Agric **15**: 1490–1498

Wang X, Liu D, Li A, Sun X, Zhang R, Wu L, Liang Y, Mao L (2013) Transcriptome analysis of tomato flower pedicel tissues reveals abscission zone-specific modulation of key meristem activity genes. PLoS One **8**: e55238

Wang Y, Li T, Meng H, Sun X (2005) Optimal and spatial analysis of hormones, degrading enzymes and isozyme profiles in tomato pedicel explants during ethylene-induced abscission. Plant Growth Regul **46**: 97–107

Wang Y, Liu R, Chen L, Wang Y, Liang Y, Wu X, Li B, Wu J, Liang Y, Wang X (2009) Nicotiana tabacum TTG1 contributes to ParA1-induced signalling and cell death in leaf trichomes. J Cell Sci **122**: 2673–2685

Wang Y, Zou W, Xiao Y, Cheng L, Liu Y, Gao S, Shi Z, Jiang Y, Qi M, Xu T, Li T (2018) MicroRNA1917 targets CTR4 splice variants to regulate ethylene responses in tomato. J Exp Bot **69**: 1011–1025

Whitelaw CA, Lyssenko NN, Chen L, Zhou D, Mattoo AK, Tucker ML (2002) Delayed abscission and shorter internodes correlate with a reduction in the ethylene receptor LeETR1 transcript in transgenic tomato. Plant Physiol **128**: 978–987

Wudick MM, Luu DT, Maurel C (2009) A look inside: localization patterns and functions of intracellular plant aquaporins. New Phytol **184**: 289–302

Xiao G, Zhao P, Zhang Y (2019) A pivotal role of hormones in regulating cotton fiber development. Front Plant Sci

Xiaosen W, Zhong D, Wenzheng Z, Zhaojiang M, Xiao C, Mouchao L, Kunbo W (2017) Effect of waterlogging duration at different growth stages on the growth, yield and quality of cotton. PLoS One **12**: e0169029

Yamasaki H, Sakihama Y, Ikehara N (1997) Flavonoid-peroxidase reaction as a detoxification mechanism of plant cells against H2O2. Plant Physiol **115**: 1405–1412

Yoo S-D, Cho YH, Sheen J (2007) Arabidopsis mesophyll protoplasts: a versatile cell system for transient gene expression analysis. Nat Protoc **2**: 1565–1572

Zeng J, Dong Z, Wu H, Tian Z, Zhao Z (2017) Redox regulation of plant stem cell fate. EMBO J **36**: 2844–2855.

Zhang RB, Verkman AS (1991) Water and urea permeability properties of Xenopus oocytes: expression of mRNA from toad urinary bladder. Am J Physiol Cell Physiol **260**: 26–34

Zhang XL, Qi MF, Xu T, Lu XJ, Li TL (2015) Proteomics profiling of ethylene-induced tomato flower pedicel abscission. J Proteomics **121**: 67–87

Zhang Y, Sa G, Zhang Y, Zhu Z, Deng S, Sun J, Li N, Li J, Yao J, Zhao N (2017) Paxillus involutus-facilitated Cd^{2+} influx through plasma membrane Ca^{2+}-permeable channels is stimulated by H_2O_2 and H^+-ATPase in ectomycorrhizal populus × canescens under cadmium stress. Front Plant Sci **7**: 1975